Scattering from a frequency selective surface supported by a bianisotropic substrate

Kristensson, Gerhard; Åkerberg, Martin; Poulsen, Sören

2000

CODEN:LUTEDX/(TEAT-7085)/1-28/(2000)

Revision No. 1: January 2001

Scattering from a frequency selective surface supported by a bianisotropic substrate

Gerhard Kristensson, Martin Åkerberg, and Sören Poulsen

Department of Electroscience
Electromagnetic Theory
Lund Institute of Technology
Sweden

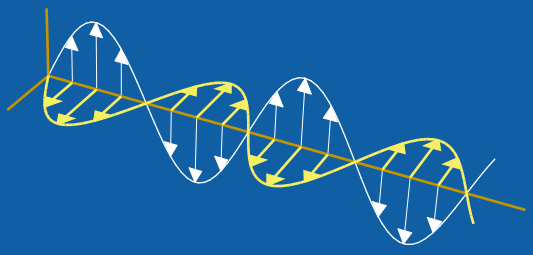

Gerhard Kristensson
Martin Åkerberg
Sören Poulsen

Department of Electroscience
Electromagnetic Theory
Lund Institute of Technology
P.O. Box 118
SE-221 00 Lund
Sweden

Editor: Gerhard Kristensson

Abstract

In this paper a method for the analysis of a frequency selective surface (FSS) supported by a bianisotropic substrate is presented. The frequency selective structure is a thin metallic pattern — the actual FSS — on a plane supporting substrate. Integral representations of the fields in combination with the method of moments carried out in the spatial Fourier domain are shown to be a fruitful way of analyzing the problem with a complex substrate. This approach results in a very general formulation in which the supporting substrate can have arbitrary bianisotropic properties. The bianisotropic slab can be homogeneous, stratified, or it can have continuously varying material parameter as a function of depth. The analysis presented in this paper is illustrated in a series of numerical examples. Results for isotropic, anisotropic and bianisotropic substrates are given.

1 Introduction

Frequency selective surfaces (FSSs), used as electromagnetic windows to affect the transmission and reflection properties for radomes, have been addressed for several decades [18, 25, 26]. For mechanical reasons, and to reduce the angular sensitivity [18, 23], it is often embedded in a dielectric medium. For isotropic slabs, the impact of the dielectric medium is traditionally taken into account by either a cascade technique [5, 6] or by using an appropriate Green's function [26]. In the cascade technique, the surface current is calculated without the substrate present. Specifically, the scattering matrices are calculated for the free-standing FSS and the substrate, respectively, and the coupling between these two structures is then determined by simple matrix algebra [26]. However, in the Green's function approach the surface current is determined in the presence of the substrate.

More complex substrates have also been addressed. Chang, Langley, and Parker report experimental results for FSSs printed on ferrite substrates [4]. The main idea is that a static magnetic field, applied on the ferrite substrate, changes the permeability of the substrate [2, 14–16]. Chiral substrates have been analyzed in Refs 7, 10, 11. In many applications, the FSS is located on a glass fiber reinforced slab. It is a well-known fact that the glass fiber reinforcement introduces anisotropic effects in the substrate, see *e.g.*, Ref. 21. Recently, uniaxial substrates were also analyzed [3].

In this paper, a method for the analysis of a frequency selective surface supported on one side by a bianisotropic substrate is presented. The bianisotropic slab is either homogeneous, stratified, or it can have continuously varying material parameters as a function of depth. The method used for the analysis is based on classical integral representations of the electromagnetic fields and the concept of wave propagators, which maps the fields from one interface to another. These wave propagators are used to obtain the reflection and transmission dyadics of the slab [22].

The present method shows several similarities with the Green's function approach cited above. The main difference is that, in the present approach, we have to calculate the reflection and transmission dyadics of the slab, while these effects in

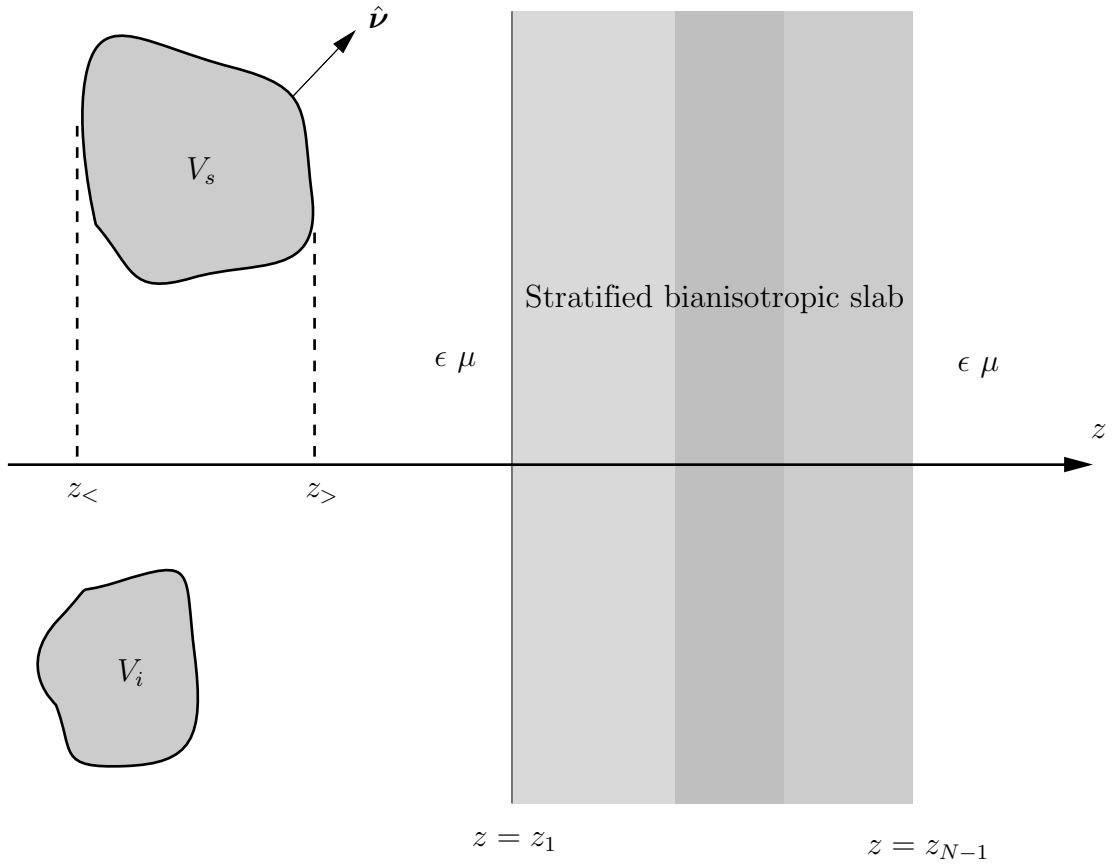

Figure 1: The geometry of the problem.

the latter approach are accounted for in the calculations of the Green's function. The main advantage of the present method is that the reflection and transmission dyadics can be calculated efficiently, even for stratified bianisotropic slabs [22].

In the derivation below, the scattering object and the incident field are first arbitrary, *e.g.*, the scatterer is of finite extent and not necessarily a thin screen. This analysis serves the purpose of being useful for a wider range of scattering problems than primarily addressed in this paper. Then, in the following section, we restrict the scatterer to be plane, perfectly conducting screen with a periodic pattern, *i.e.*, the scatterer is a FSS. Moreover, the incident field is restricted to be a plane wave. Finally, in Section 5, the analysis presented in this paper is illustrated in a series of numerical examples. Results for isotropic, uniaxial, and bianisotropic substrates are given. Moreover, results for a tripole loop FSS are presented. Predicted and measured power reflection are compared and excellent agreement is found.

2 General case — arbitrary scatterer

The geometry of interest in this paper is depicted in Figure 1. The sources of the problem are assumed to be confined to a region V_i (may be at infinity) located to the

left of the slab, which extends from $z = z_1$ to $z = z_{N-1}$. The depth parameter z is defined by the normal of the interfaces as shown in the figure. The bianisotropic slab is either homogeneous, stratified, or it can can have continuously varying material parameters as a function of depth. In the lateral directions, however, there are no variations in the material parameters. The scatterer — at this stage a finite scatterer — is confined to the volume V_s. This volume is located to the left of the slab and no parts are intersecting the slab. Moreover, we denote the leftmost (rightmost) position of the scattering region by $z_<$ ($z_>$). The source region, V_i, does not intersect the scatterer, V_s, or the slab. The space outside the slab and the source and scattering regions is assumed to be homogeneous and isotropic with relative permittivity ϵ and permeability μ, *i.e.*, ϵ and μ are constants. In all practical situations of interest in technical applications, these spaces are lossless, *i.e.*, ϵ and μ are real numbers.[1]

This geometry can be relaxed in various ways, *e.g.*, we can have additional sources and the scatterers located on the right hand side of the slab. Such generalizations change the result of this paper in several details, but they do not alter the basic methods we apply to solve this class of scattering problems. We can also treat a more complex situation with bianisotropic slabs on both sides of the scatterer. These generalizations will be addressed in a subsequent paper.

We start with a review of the basic equations needed for the analysis in this paper. In Section 2.1, we review and apply the integral representation of the electric field in an isotropic medium, and in Section 2.2, we review and apply the plane vector wave decomposition of the Green's dyadic for an isotropic medium.

2.1 Integral representation in an isotropic medium

The integral representation of the solution to the Maxwell equations in an isotropic region, characterized by the relative permittivity ϵ and permeability μ, and bounded by the closed surface S (outwardly directed normal $\hat{\boldsymbol{\nu}}$) is [24]

$$\begin{aligned} &-i\frac{\eta_0\eta}{k}\nabla\times\left\{\nabla\times\iint\limits_S \mathbf{G}(k,|\boldsymbol{r}-\boldsymbol{r}'|)\cdot(\hat{\boldsymbol{\nu}}(\boldsymbol{r}')\times\boldsymbol{H}(\boldsymbol{r}'))\,dS'\right\} \\ &-\nabla\times\iint\limits_S \mathbf{G}(k,|\boldsymbol{r}-\boldsymbol{r}'|)\cdot(\hat{\boldsymbol{\nu}}(\boldsymbol{r}')\times\boldsymbol{E}(\boldsymbol{r}'))\,dS' = \begin{cases}\boldsymbol{E}(\boldsymbol{r}), & \boldsymbol{r}\text{ inside }S\\ \mathbf{0}, & \boldsymbol{r}\text{ outside }S\end{cases} \end{aligned} \tag{2.1}$$

where the Green's dyadic in an isotropic region is

$$\mathbf{G}(k,r) = \mathbf{I}_3\frac{e^{ikr}}{4\pi r} \tag{2.2}$$

[1]This assumption is not of vital importance in the treatment below, and it can easily be relaxed. It is only of importance in the computations of the reflectance and the transmittance of the structure, since we then are calculating the field far away from the slab. Moreover, it is possible to have different material parameters to the left of the slab, $z < z_1$, and to the right of the slab, $z > z_{N-1}$.

where $k = k_0 (\epsilon\mu)^{1/2}$ is the wave number, $\eta = \sqrt{\mu/\epsilon}$ is the relative wave impedance, and $k_0 = \omega/c_0$ and η_0 are the wave number and the wave impedance of vacuum, respectively. Notice that this Green's dyadic is a product of the identity dyadic in three spatial dimensions, $\mathbf{I}_3$, and the Green's function of the scalar Helmholtz equation. Therefore, it contains a part that is not solenoidal [17]. The lower part of this integral representation in (2.1) is usually referred to as the extinction theorem.

The field from the source region, V_i, without the influence of the slab or the scatterer is denoted $\boldsymbol{E}^i$. The presence of the slab and the scatterer alters this field by the scattered field $\boldsymbol{E}^s$. The total field $\boldsymbol{E}$ is

$$\boldsymbol{E} = \boldsymbol{E}^i + \boldsymbol{E}^s$$

A similar notation is used for the magnetic field $\boldsymbol{H}$.

We now apply the integral representation in (2.1) to the geometry in Figure 1. Specifically, we get for a volume V that consists of the space to the left of the slab and outside the source and scattering regions (this result is actually the limit as the radius goes to infinity from a contribution of a large half sphere in the left half space, where the fields are assumed to satisfy appropriate radiation conditions)

$$\begin{aligned}
&i\frac{\eta_0\eta}{k}\nabla\times\left\{\nabla\times\iint\limits_{S_s}\mathbf{G}(k,|\boldsymbol{r}-\boldsymbol{r}'|)\cdot(\hat{\boldsymbol{\nu}}(\boldsymbol{r}')\times\boldsymbol{H}(\boldsymbol{r}'))\;dS'\right\}\\
&+\nabla\times\iint\limits_{S_s}\mathbf{G}(k,|\boldsymbol{r}-\boldsymbol{r}'|)\cdot(\hat{\boldsymbol{\nu}}(\boldsymbol{r}')\times\boldsymbol{E}(\boldsymbol{r}'))\;dS'\\
&-i\frac{\eta_0\eta}{k}\nabla\times\left\{\nabla\times\iint\limits_{z'=z_1}\mathbf{G}(k,|\boldsymbol{r}-\boldsymbol{r}'|)\cdot(\hat{\boldsymbol{z}}\times\boldsymbol{H}(\boldsymbol{r}'))\;dx'y'\right\}\\
&-\nabla\times\iint\limits_{z'=z_1}\mathbf{G}(k,|\boldsymbol{r}-\boldsymbol{r}'|)\cdot(\hat{\boldsymbol{z}}\times\boldsymbol{E}(\boldsymbol{r}'))\;dx'y'\\
&\quad=\begin{cases}\boldsymbol{E}^s(\boldsymbol{r}), & z<z_1 \text{ and } \boldsymbol{r} \text{ outside } S_s\\ -\boldsymbol{E}^i(\boldsymbol{r}), & \boldsymbol{r} \text{ inside } S_s \text{ or } z>z_1\end{cases}
\end{aligned}\tag{2.3}$$

where the limits of the fields in the surface integrals are taken as limit values from the isotropic region, *i.e.*, from the outside of the scatterer and from $z = z_1 - 0$. The unit normal of the scatterer, $\hat{\boldsymbol{\nu}}$, is directed outwards into the isotropic medium as denoted in Figure 1.

These expressions give a representation of the scattered electric field, $\boldsymbol{E}^s$, outside the scatterer (and to the left of the slab), and a representation of the incident field, $\boldsymbol{E}^i$, inside the scatterer or inside the slab. The associated magnetic fields are easily found by the Faraday's law

$$\boldsymbol{H}(\boldsymbol{r}) = \frac{1}{ik\eta\eta_0}\nabla\times\boldsymbol{E}(\boldsymbol{r})$$

2.2 Plane wave expansion of the Green's dyadic

In a geometry where the medium is laterally homogeneous, it is natural to decompose the fields in a spectrum of plane waves, *i.e.*, a Fourier transformation of the fields with respect to the lateral variable $\boldsymbol{\rho} = \hat{\boldsymbol{x}}x + \hat{\boldsymbol{y}}y$. The Fourier transform of a time-harmonic field $\boldsymbol{E}(\boldsymbol{r})$ is defined by

$$\boldsymbol{E}(\boldsymbol{k}_t, z) = \iint_{-\infty}^{\infty} \boldsymbol{E}(\boldsymbol{r}) e^{-i\boldsymbol{k}_t \cdot \boldsymbol{\rho}} \, dx \, dy$$

where

$$\boldsymbol{k}_t = \hat{\boldsymbol{x}}k_x + \hat{\boldsymbol{y}}k_y$$

is the transverse (tangential) wave vector and

$$k_t = \sqrt{k_x^2 + k_y^2}$$

the transverse (tangential) wave number. The inverse Fourier transform is defined by

$$\boldsymbol{E}(\boldsymbol{r}) = \frac{1}{4\pi^2} \iint_{-\infty}^{\infty} \boldsymbol{E}(\boldsymbol{k}_t, z) e^{i\boldsymbol{k}_t \cdot \boldsymbol{\rho}} \, dk_x \, dk_y \tag{2.4}$$

Notice that, in order to avoid cumbersome notation, the same letter is used to denote the Fourier transform of the field and the field itself. The argument of the field shows what field is intended.

Moreover, the normal (longitudinal) wave number, k_z, is defined by

$$k_z = \left(k^2 - k_t^2\right)^{1/2} = \begin{cases} \sqrt{k^2 - k_t^2} \text{ for } k_t < k \\ i\sqrt{k_t^2 - k^2} \text{ for } k_t > k \end{cases}$$

The pertinent expansion (Weyl's expansion) of the Green's dyadic in a homogeneous, isotropic medium, (2.2), is [1][2]

$$\begin{aligned} \mathbf{G}(k; |\boldsymbol{r} - \boldsymbol{r}'|) &= \frac{i}{8\pi^2} \sum_{j=1}^{3} \iint_{-\infty}^{\infty} \hat{\boldsymbol{e}}_j^+ \hat{\boldsymbol{e}}_j^+ e^{i\boldsymbol{k}_t \cdot (\boldsymbol{\rho} - \boldsymbol{\rho}') + ik_z |z - z'|} \frac{dk_x \, dk_y}{k_z} \\ &= \frac{i}{8\pi^2} \sum_{j=1}^{3} \iint_{-\infty}^{\infty} \hat{\boldsymbol{e}}_j^- \hat{\boldsymbol{e}}_j^- e^{i\boldsymbol{k}_t \cdot (\boldsymbol{\rho} - \boldsymbol{\rho}') + ik_z |z - z'|} \frac{dk_x \, dk_y}{k_z} \end{aligned} \tag{2.5}$$

[2]The Fourier transform $\mathbf{G}(k; \boldsymbol{k}_t, z) = -\mathbf{I}_3 \frac{e^{ik_z|z|}}{2ik_z}$ of $\mathbf{G}(k; r)$ w.r.t. $\boldsymbol{\rho}$ satisfies the ODE

$$-\left(\frac{d^2}{dz^2} + k_z^2\right) \mathbf{G}(k; \boldsymbol{k}_t, z) = \mathbf{I}_3 \delta(z);$$

therefore,

$$\mathbf{G}(k; r) = \frac{1}{4\pi^2} \iint_{-\infty}^{\infty} \mathbf{G}(k; \boldsymbol{k}_t, z) e^{i\boldsymbol{k}_t \cdot \boldsymbol{\rho}} \, dk_x \, dk_y = \frac{1}{4\pi^2} \iint_{-\infty}^{\infty} \left(-\mathbf{I}_3 \frac{e^{ik_z|z|}}{2ik_z}\right) e^{i\boldsymbol{k}_t \cdot \boldsymbol{\rho}} \, dk_x \, dk_y$$

where the (complex) unit vectors $\hat{\boldsymbol{e}}_j^{\pm}$, $j = 1, 2, 3$, are defined as[3] ($k_t \neq 0$):

$$\begin{cases} \hat{\boldsymbol{e}}_1^{\pm} = \hat{\boldsymbol{e}}_2^{\pm} \times \hat{\boldsymbol{e}}_3^{\pm} = \dfrac{\pm \boldsymbol{k}_t k_z - k_t^2 \hat{\boldsymbol{z}}}{k k_t} = \pm \dfrac{k_z}{k} \hat{\boldsymbol{e}}_{\parallel} - \dfrac{k_t}{k} \hat{\boldsymbol{z}} \\ \hat{\boldsymbol{e}}_2^{\pm} = \dfrac{\hat{\boldsymbol{z}} \times \hat{\boldsymbol{e}}_3^{\pm}}{\left| \hat{\boldsymbol{z}} \times \hat{\boldsymbol{e}}_3^{\pm} \right|} = \dfrac{\hat{\boldsymbol{z}} \times \boldsymbol{k}_t}{k_t} = \dfrac{-k_y \hat{\boldsymbol{x}} + k_x \hat{\boldsymbol{y}}}{k_t} = \hat{\boldsymbol{e}}_{\perp} \\ \hat{\boldsymbol{e}}_3^{\pm} = \dfrac{\boldsymbol{k}_t \pm \hat{\boldsymbol{z}} k_z}{k} = \hat{\boldsymbol{e}}_{\parallel} \dfrac{k_t}{k} \pm \dfrac{k_z}{k} \hat{\boldsymbol{z}} \end{cases}$$

where we have introduced two (real) unit vectors in the x-y-plane:

$$\begin{cases} \hat{\boldsymbol{e}}_{\parallel}(\boldsymbol{k}_t) = \boldsymbol{k}_t / k_t \\ \hat{\boldsymbol{e}}_{\perp}(\boldsymbol{k}_t) = \hat{\boldsymbol{z}} \times \hat{\boldsymbol{e}}_{\parallel}(\boldsymbol{k}_t) \end{cases}$$

The plane vector waves are denoted $\hat{\boldsymbol{e}}_j^{\pm} e^{i\boldsymbol{k}_t \cdot \boldsymbol{\rho} \pm i k_z z}$, $j = 1, 2, 3$. The upper (lower) sign refers to the right- (left-) going plane vector waves. We refrain from introducing a special notation for these plane vector waves, since the analysis in this paper does only use the unit vectors $\hat{\boldsymbol{e}}_j^{\pm}$, $j = 1, 2, 3,$. This is contrast to the analysis made in Refs [9, 12, 13]. The decomposition of the Green's dyadic in (2.5) is in plane vector waves.

Moreover, the complex unit vector $\hat{\boldsymbol{e}}_1^{\pm}(\boldsymbol{k}_t)$ is constructed from $\hat{\boldsymbol{e}}_{\parallel}(\boldsymbol{k}_t)$ by the dyadic $\boldsymbol{\gamma}^{\pm}(\boldsymbol{k}_t)$. Specifically, we have

$$\hat{\boldsymbol{e}}_1^{\pm} = \frac{k_z}{k} \boldsymbol{\gamma}^{\pm} \cdot \hat{\boldsymbol{e}}_{\parallel}$$

where

$$\boldsymbol{\gamma}^{\pm}(\boldsymbol{k}_t) = \pm \left(\mathbf{I}_2 \mp \frac{k_t}{k_z} \hat{\boldsymbol{z}} \hat{\boldsymbol{e}}_{\parallel} \right) \tag{2.6}$$

where $\mathbf{I}_2$ is the identity dyadic in the x-y-plane. In addition, this dyadic is used to reconstruct the z-component of a tangential field, see also Section 2.4.

The unit vectors $\hat{\boldsymbol{e}}_j^{\pm}$, $j = 1, 2, 3$, are the spherical basis functions associated with the complex vector $\boldsymbol{k}_t \pm \hat{\boldsymbol{z}} k_z$, *i.e.*, they form a right-hand oriented set of basis vectors. Index $j = 1$ denotes TM-fields and $j = 2$ denotes TE-fields. Index $j = 3$ does not enter into our analysis due to the fact that the electric and magnetic fields are solenoidal. From these definitions we easily see that

$$\begin{cases} \nabla \times \hat{\boldsymbol{e}}_1^{\pm} e^{i\boldsymbol{k}_t \cdot \boldsymbol{\rho} \pm i k_z z} = ik \hat{\boldsymbol{e}}_2^{\pm} e^{i\boldsymbol{k}_t \cdot \boldsymbol{\rho} \pm i k_z z} = ik \hat{\boldsymbol{e}}_{\bar{1}}^{\pm} e^{i\boldsymbol{k}_t \cdot \boldsymbol{\rho} \pm i k_z z} \\ \nabla \times \hat{\boldsymbol{e}}_2^{\pm} e^{i\boldsymbol{k}_t \cdot \boldsymbol{\rho} \pm i k_z z} = -ik \hat{\boldsymbol{e}}_1^{\pm} e^{i\boldsymbol{k}_t \cdot \boldsymbol{\rho} \pm i k_z z} = -ik \hat{\boldsymbol{e}}_{\bar{2}}^{\pm} e^{i\boldsymbol{k}_t \cdot \boldsymbol{\rho} \pm i k_z z} \\ \nabla \times \hat{\boldsymbol{e}}_3^{\pm} e^{i\boldsymbol{k}_t \cdot \boldsymbol{\rho} \pm i k_z z} = \mathbf{0} \end{cases}$$

where we have introduced the dual index $\bar{1} = 2$ and $\bar{2} = 1$. From these results, and the fact that the integral representations in (2.3) always contain a curl operator

[3] These vectors originate from $\mathbf{I}_3 = \boldsymbol{k}_t \boldsymbol{k}_t / k_t^2 + (\hat{\boldsymbol{z}} \times \boldsymbol{k}_t)(\hat{\boldsymbol{z}} \times \boldsymbol{k}_t) / k_t^2 + \hat{\boldsymbol{z}} \hat{\boldsymbol{z}} = \sum_{j=1}^{3} \hat{\boldsymbol{e}}_j^{+} \hat{\boldsymbol{e}}_j^{+} = \sum_{j=1}^{3} \hat{\boldsymbol{e}}_j^{-} \hat{\boldsymbol{e}}_j^{-}$ which is a decomposition of the unit dyadic in cylindrical coordinates.

in front of the integrals, we see that $j = 3$ does not enter in this electromagnetic application. The summation in (2.5) is therefore effectively over $j = 1, 2$.

In this paper, we work in a dyadic notation. Several dyadics are important in this context. The symmetric projection dyadic $\mathbf{P}^{\pm}(\boldsymbol{k}_t)$ defined by

$$\mathbf{P}^{\pm}(\boldsymbol{k}_t) = \mathbf{I}_3 - \hat{\boldsymbol{e}}_3^{\pm}(\boldsymbol{k}_t)\hat{\boldsymbol{e}}_3^{\pm}(\boldsymbol{k}_t) = \frac{k_z^2}{k^2}\hat{\boldsymbol{e}}_{\parallel}\hat{\boldsymbol{e}}_{\parallel} + \hat{\boldsymbol{e}}_{\perp}\hat{\boldsymbol{e}}_{\perp} \mp \frac{k_t k_z}{k^2}\left(\hat{\boldsymbol{z}}\hat{\boldsymbol{e}}_{\parallel} + \hat{\boldsymbol{e}}_{\parallel}\hat{\boldsymbol{z}}\right) + \frac{k_t^2}{k^2}\hat{\boldsymbol{z}}\hat{\boldsymbol{z}} \quad (2.7)$$

projects out the divergence-free (solenoidal) parts of any vector, *i.e.*, the $j = 1, 2$ parts. We also have use for the x-y-part of this projector. To this end, we define

$$\boldsymbol{\Gamma}(\boldsymbol{k}_t) = \frac{k_z^2}{k^2}\hat{\boldsymbol{e}}_{\parallel}\hat{\boldsymbol{e}}_{\parallel} + \hat{\boldsymbol{e}}_{\perp}\hat{\boldsymbol{e}}_{\perp} = \frac{k^2\mathbf{I}_2 - \boldsymbol{k}_t\boldsymbol{k}_t}{k^2}$$

which also can be written as

$$\boldsymbol{\Gamma}(\boldsymbol{k}_t) = (\mathbf{I}_3 - \hat{\boldsymbol{z}}\hat{\boldsymbol{z}}) \cdot \mathbf{P}^{\pm}(\boldsymbol{k}_t) \cdot (\mathbf{I}_3 - \hat{\boldsymbol{z}}\hat{\boldsymbol{z}}) = \mathbf{I}_2 \cdot \mathbf{P}^{\pm}(\boldsymbol{k}_t) \cdot \mathbf{I}_2$$

Note also that the projection dyadic $\mathbf{P}^{\pm}$ can be expressed in the dyadic $\boldsymbol{\gamma}^{\pm}$ in (2.6). The result is

$$\mathbf{P}^{\pm} = \frac{k_z^2}{k^2}\boldsymbol{\gamma}^{\pm} \cdot (\boldsymbol{\gamma}^{\pm})^t + \frac{k_t^2}{k^2}\hat{\boldsymbol{e}}_{\perp}\hat{\boldsymbol{e}}_{\perp}$$

where superscript $()^t$ denotes the transpose of the dyadic.

We also introduce the rotated dyadic $\mathbf{Q}^{\pm}(\boldsymbol{k}_t)$ defined by

$$\begin{aligned} \mathbf{Q}^{\pm}(\boldsymbol{k}_t) &= \mathbf{P}^{\pm}(\boldsymbol{k}_t) \times \hat{\boldsymbol{e}}_3^{\pm}(\boldsymbol{k}_t) = \hat{\boldsymbol{e}}_2^{\pm}(\boldsymbol{k}_t)\hat{\boldsymbol{e}}_1^{\pm}(\boldsymbol{k}_t) - \hat{\boldsymbol{e}}_1^{\pm}(\boldsymbol{k}_t)\hat{\boldsymbol{e}}_2^{\pm}(\boldsymbol{k}_t) \\ &= \pm\frac{k_z}{k}\left(\hat{\boldsymbol{e}}_{\perp}\hat{\boldsymbol{e}}_{\parallel} - \hat{\boldsymbol{e}}_{\parallel}\hat{\boldsymbol{e}}_{\perp}\right) - \frac{k_t}{k}\left(\hat{\boldsymbol{e}}_{\perp}\hat{\boldsymbol{z}} - \hat{\boldsymbol{z}}\hat{\boldsymbol{e}}_{\perp}\right) \end{aligned} \quad (2.8)$$

Note that this dyadic is anti-symmetric.

These projection dyadics are useful in expressing the curl of the Green's dyadic in (2.5), *viz.*,

$$\begin{cases} \nabla \times \mathbf{G}(k; |\boldsymbol{r} - \boldsymbol{r}'|) = -\dfrac{k}{8\pi^2}\displaystyle\iint_{-\infty}^{\infty} \mathbf{Q}^{\pm}(\boldsymbol{k}_t) e^{i\boldsymbol{k}_t\cdot(\boldsymbol{\rho}-\boldsymbol{\rho}')+ik_z|z-z'|}\frac{dk_x\,dk_y}{k_z} \\ \nabla \times (\nabla \times \mathbf{G}(k; |\boldsymbol{r} - \boldsymbol{r}'|)) = \dfrac{ik^2}{8\pi^2}\displaystyle\iint_{-\infty}^{\infty} \mathbf{P}^{\pm}(\boldsymbol{k}_t) e^{i\boldsymbol{k}_t\cdot(\boldsymbol{\rho}-\boldsymbol{\rho}')+ik_z|z-z'|}\frac{dk_x\,dk_y}{k_z} \end{cases}$$

2.3 Expansion relations

In this section, we apply the result of Section 2.2 to the integral representation (2.3) in Section 2.1.

For a point $\boldsymbol{r}$ such that $z_> < z < z_1$, *i.e.*, between the scatterer and the slab, see Figure 1, we get

$$\boldsymbol{E}^s(\boldsymbol{r}) = \frac{1}{4\pi^2}\iint_{-\infty}^{\infty} \boldsymbol{\alpha}(\boldsymbol{k}_t) e^{i\boldsymbol{k}_t\cdot\boldsymbol{\rho}+ik_z z}\,dk_x\,dk_y + \frac{1}{4\pi^2}\iint_{-\infty}^{\infty} \boldsymbol{\beta}(\boldsymbol{k}_t) e^{i\boldsymbol{k}_t\cdot\boldsymbol{\rho}-ik_z z}\,dk_x\,dk_y \quad (2.9)$$

where

$$\begin{cases} \boldsymbol{\alpha}(\boldsymbol{k}_t) = -\dfrac{k}{2k_z}\Bigg\{\mathbf{P}^+(\boldsymbol{k}_t)\cdot\iint\limits_{S_s}\left(\hat{\boldsymbol{\nu}}(\boldsymbol{r}')\times\eta_0\eta\boldsymbol{H}(\boldsymbol{r}')\right)e^{-i\boldsymbol{k}_t\cdot\boldsymbol{\rho}'-ik_z z'}\,dS' \\ \qquad\qquad + \mathbf{Q}^+(\boldsymbol{k}_t)\cdot\iint\limits_{S_s}\left(\hat{\boldsymbol{\nu}}(\boldsymbol{r}')\times\boldsymbol{E}(\boldsymbol{r}')\right)e^{-i\boldsymbol{k}_t\cdot\boldsymbol{\rho}'-ik_z z'}\,dS'\Bigg\} \\ \boldsymbol{\beta}(\boldsymbol{k}_t) = \dfrac{k}{2k_z}\left\{\mathbf{P}^-(\boldsymbol{k}_t)\cdot(\hat{\boldsymbol{z}}\times\eta_0\eta\boldsymbol{H}(\boldsymbol{k}_t,z_1)) + \mathbf{Q}^-(\boldsymbol{k}_t)\cdot(\hat{\boldsymbol{z}}\times\boldsymbol{E}(\boldsymbol{k}_t,z_1))\right\}e^{ik_z z_1} \end{cases} \tag{2.10}$$

where $\boldsymbol{E}(\boldsymbol{k}_t, z_1)$ and $\boldsymbol{H}(\boldsymbol{k}_t, z_1)$ denotes the Fourier transformed field over the interface $z = z_1$. This expression of the scattered field between the scatterer and the slab is a decomposition of the field into right- and left-going plane vector waves.

The great advantage with the approach used here is that we have an exact relation between the expansion coefficients, $\boldsymbol{\alpha}(\boldsymbol{k}_t)$ and $\boldsymbol{\beta}(\boldsymbol{k}_t)$, and the surface fields on S_s, $\boldsymbol{E}$ and $\boldsymbol{H}$, and the Fourier transformed fields, $\boldsymbol{E}(\boldsymbol{k}_t, z_1)$ and $\boldsymbol{H}(\boldsymbol{k}_t, z_1)$, on $z = z_1$. These relations, and the analogous relations below, are in fact the key to the solution of the entire scattering problem.

Similarly, for a point $\boldsymbol{r}$ such that $z < z_<$, *i.e.*, to the left of the scatterer, we get

$$\boldsymbol{E}^s(\boldsymbol{r}) = \frac{1}{4\pi^2}\iint\limits_{-\infty}^{\infty}\boldsymbol{f}(\boldsymbol{k}_t)e^{i\boldsymbol{k}_t\cdot\boldsymbol{\rho}-ik_z z}\,dk_x\,dk_y \tag{2.11}$$

where

$$\begin{aligned} \boldsymbol{f}(\boldsymbol{k}_t) = -\frac{k}{2k_z}\Bigg\{&\mathbf{P}^-(\boldsymbol{k}_t)\cdot\iint\limits_{S_s}\left(\hat{\boldsymbol{\nu}}(\boldsymbol{r}')\times\eta_0\eta\boldsymbol{H}(\boldsymbol{r}')\right)e^{-i\boldsymbol{k}_t\cdot\boldsymbol{\rho}'+ik_z z'}\,dS' \\ &+ \mathbf{Q}^-(\boldsymbol{k}_t)\cdot\iint\limits_{S_s}\left(\hat{\boldsymbol{\nu}}(\boldsymbol{r}')\times\boldsymbol{E}(\boldsymbol{r}')\right)e^{-i\boldsymbol{k}_t\cdot\boldsymbol{\rho}'+ik_z z'}\,dS'\Bigg\} \\ &+ \frac{k}{2k_z}\left\{\mathbf{P}^-(\boldsymbol{k}_t)\cdot(\hat{\boldsymbol{z}}\times\eta_0\eta\boldsymbol{H}(\boldsymbol{k}_t,z_1)) + \mathbf{Q}^-(\boldsymbol{k}_t)\cdot(\hat{\boldsymbol{z}}\times\boldsymbol{E}(\boldsymbol{k}_t,z_1))\right\}e^{ik_z z_1} \end{aligned} \tag{2.12}$$

This expression is a representation of the scattered (reflected) field to the left of the scattering region. This representation contains only left-going plane vector wave, due to the fact that all scatterer lie to the right of the observation point. Notice that this intuitive result is obtained by a systematic use of the integral representation and a decomposition of the Green's dyadic in plane vector waves.

Moreover, for a point $\boldsymbol{r}$ such that $z > z_1$ we get an expansion of the incident field $\boldsymbol{E}^i$. The result is

$$\boldsymbol{E}^i(\boldsymbol{r}) = \frac{1}{4\pi^2}\iint\limits_{-\infty}^{\infty}\boldsymbol{a}(\boldsymbol{k}_t)e^{i\boldsymbol{k}_t\cdot\boldsymbol{\rho}+ik_z z}\,dk_x\,dk_y \tag{2.13}$$

where

$$\boldsymbol{a}(\boldsymbol{k}_t) = \frac{k}{2k_z}\Bigg\{\mathbf{P}^+(\boldsymbol{k}_t)\cdot\iint\limits_{S_s}\left(\hat{\boldsymbol{\nu}}(\boldsymbol{r}')\times\eta_0\eta\boldsymbol{H}(\boldsymbol{r}')\right)e^{-i\boldsymbol{k}_t\cdot\boldsymbol{\rho}'-ik_z z'}\,dS' \\ + \mathbf{Q}^+(\boldsymbol{k}_t)\cdot\iint\limits_{S_s}\left(\hat{\boldsymbol{\nu}}(\boldsymbol{r}')\times\boldsymbol{E}(\boldsymbol{r}')\right)e^{-i\boldsymbol{k}_t\cdot\boldsymbol{\rho}'-ik_z z'}\,dS'\Bigg\} \\ -\frac{k}{2k_z}\left\{\mathbf{P}^+(\boldsymbol{k}_t)\cdot(\hat{\boldsymbol{z}}\times\eta_0\eta\boldsymbol{H}(\boldsymbol{k}_t,z_1))+\mathbf{Q}^+(\boldsymbol{k}_t)\cdot(\hat{\boldsymbol{z}}\times\boldsymbol{E}(\boldsymbol{k}_t,z_1))\right\}e^{-ik_z z_1} \tag{2.14}$$

This is a decomposition of the incident field to the right of the source region, therefore, the expansion only contains right-going plane vector waves. Since the incident field is given, $\boldsymbol{a}(\boldsymbol{k}_t)$ is a known quantity.

2.4 Propagation in the stratified region

The Fourier transform of the fields at the interface $z = z_1$ and the fields at $z = z_{N-1}$ are related [22]. As a first step in finding this relation, we introduce a wave-splitting technique that decomposes any Fourier transformed field into two components that transport power in the $+z$- or the $-z$-directions, respectively. The wave-splitting technique in a homogeneous, isotropic medium and the concept of wave propagators is presented in detail in *e.g.*, [22]. We have

$$\begin{pmatrix}\boldsymbol{E}_{xy}(\boldsymbol{k}_t,z)\\ \eta\eta_0\hat{\boldsymbol{z}}\times\boldsymbol{H}_{xy}(\boldsymbol{k}_t,z)\end{pmatrix} = \begin{pmatrix}\mathbf{I}_2 & \mathbf{I}_2\\ -\mathbf{O}^{-1}(\boldsymbol{k}_t) & \mathbf{O}^{-1}(\boldsymbol{k}_t)\end{pmatrix}\cdot\begin{pmatrix}\boldsymbol{F}^+(\boldsymbol{k}_t,z)\\ \boldsymbol{F}^-(\boldsymbol{k}_t,z)\end{pmatrix} \tag{2.15}$$

where

$$\mathbf{O}^{-1} = \frac{k}{k_z}\left(\mathbf{I}_2+\frac{1}{k^2}\boldsymbol{k}_t\times(\boldsymbol{k}_t\times\mathbf{I}_2)\right) = \hat{\boldsymbol{e}}_\parallel\hat{\boldsymbol{e}}_\parallel\frac{k}{k_z}+\hat{\boldsymbol{e}}_\perp\hat{\boldsymbol{e}}_\perp\frac{k_z}{k} \tag{2.16}$$

where, as above, $\mathbf{I}_2$ is the identity dyadic in the x-y-plane. The inverse of this dyadic in the x-y-plane is

$$\mathbf{O} = \frac{k_z}{k}\left(\mathbf{I}_2-\frac{1}{k_z^2}\boldsymbol{k}_t\times(\boldsymbol{k}_t\times\mathbf{I}_2)\right) = \hat{\boldsymbol{e}}_\parallel\hat{\boldsymbol{e}}_\parallel\frac{k_z}{k}+\hat{\boldsymbol{e}}_\perp\hat{\boldsymbol{e}}_\perp\frac{k}{k_z} = \frac{k}{k_z}\mathbf{I}_2-\frac{k_t^2}{kk_z}\hat{\boldsymbol{e}}_\parallel\hat{\boldsymbol{e}}_\parallel$$

and we have

$$\begin{pmatrix}\boldsymbol{F}^+(\boldsymbol{k}_t,z)\\ \boldsymbol{F}^-(\boldsymbol{k}_t,z)\end{pmatrix} = \frac{1}{2}\begin{pmatrix}\mathbf{I}_2 & -\mathbf{O}(\boldsymbol{k}_t)\\ \mathbf{I}_2 & \mathbf{O}(\boldsymbol{k}_t)\end{pmatrix}\cdot\begin{pmatrix}\boldsymbol{E}_{xy}(\boldsymbol{k}_t,z)\\ \eta\eta_0\hat{\boldsymbol{z}}\times\boldsymbol{H}_{xy}(\boldsymbol{k}_t,z)\end{pmatrix} \tag{2.17}$$

To see the physical implications of this transformation, we proceed by eliminating the transverse magnetic field $\boldsymbol{H}_{xy}(\boldsymbol{k}_t,z)$ in order to get an expression that involves only the transverse electric field $\boldsymbol{E}_{xy}(\boldsymbol{k}_t,z)$ on the right hand side. In a homogeneous, isotropic region the electric and the magnetic fields are related by

$$k\eta\eta_0\boldsymbol{H}(\boldsymbol{k}_t,z) = \boldsymbol{k}_t\times\boldsymbol{E}(\boldsymbol{k}_t,z)\pm k_z\hat{\boldsymbol{z}}\times\boldsymbol{E}(\boldsymbol{k}_t,z)$$

depending on whether the z-dependence is $\exp\{ik_z z\}$ (upper sign) or $\exp\{-ik_z z\}$ (lower sign), respectively. From this relation we get

$$\begin{aligned} k\eta\eta_0 \hat{\boldsymbol{z}} \times \boldsymbol{H}_{xy}(\boldsymbol{k}_t, z) &= \boldsymbol{k}_t E_z(\boldsymbol{k}_t, z) \mp k_z \boldsymbol{E}_{xy}(\boldsymbol{k}_t, z) \\ &= \mp \left(\frac{1}{k_z} \boldsymbol{k}_t \left(\boldsymbol{k}_t \cdot \boldsymbol{E}_{xy}(\boldsymbol{k}_t, z) \right) + k_z \boldsymbol{E}_{xy}(\boldsymbol{k}_t, z) \right) \end{aligned} \tag{2.18}$$

where we have used $\nabla \cdot \boldsymbol{E}(\boldsymbol{r}) = 0$ to eliminate the z-component of the electric field. From this and (2.17) we get

$$\begin{cases} \boldsymbol{F}^+(\boldsymbol{k}_t, z) = \dfrac{1}{2} \boldsymbol{E}_{xy}(\boldsymbol{k}_t, z) \pm \dfrac{1}{2k} \mathbf{O}(\boldsymbol{k}_t) \cdot \left(\dfrac{1}{k_z} \boldsymbol{k}_t \left(\boldsymbol{k}_t \cdot \boldsymbol{E}_{xy}(\boldsymbol{k}_t, z) \right) + k_z \boldsymbol{E}_{xy}(\boldsymbol{k}_t, z) \right) \\ \boldsymbol{F}^-(\boldsymbol{k}_t, z) = \dfrac{1}{2} \boldsymbol{E}_{xy}(\boldsymbol{k}_t, z) \mp \dfrac{1}{2k} \mathbf{O}(\boldsymbol{k}_t) \cdot \left(\dfrac{1}{k_z} \boldsymbol{k}_t \left(\boldsymbol{k}_t \cdot \boldsymbol{E}_{xy}(\boldsymbol{k}_t, z) \right) + k_z \boldsymbol{E}_{xy}(\boldsymbol{k}_t, z) \right) \end{cases}$$

or

$$\begin{cases} \boldsymbol{F}^+(\boldsymbol{k}_t, z) = \left(\dfrac{1}{2} \pm \dfrac{1}{2} \right) \boldsymbol{E}_{xy}(\boldsymbol{k}_t, z) = \begin{cases} \boldsymbol{E}_{xy}(\boldsymbol{k}_t, z) & (\exp\{ik_z z\}) \\ \mathbf{0} & (\exp\{-ik_z z\}) \end{cases} \\ \boldsymbol{F}^-(\boldsymbol{k}_t, z) = \left(\dfrac{1}{2} \mp \dfrac{1}{2} \right) \boldsymbol{E}_{xy}(\boldsymbol{k}_t, z) = \begin{cases} \mathbf{0} & (\exp\{ik_z z\}) \\ \boldsymbol{E}_{xy}(\boldsymbol{k}_t, z) & (\exp\{-ik_z z\}) \end{cases} \end{cases}$$

From this derivation we see that the upper (lower) sign, which has an $\exp\{ik_z z\}$ ($\exp\{-ik_z z\}$) dependence, represents the part of the field that transports the power to the right (left). In fact, if the evanescent wave contribution is neglected, the power flow (Poynting's vector), averaged over a plane $z =$ constant, see (A.2), is

$$\begin{aligned} &\int_{-\infty}^{\infty}\!\!\int \hat{\boldsymbol{z}} \cdot \boldsymbol{S}(\boldsymbol{r})\, dx\, dy \\ &\quad = \frac{1}{8\pi^2 \eta\eta_0} \iint_{k_t \le k} \frac{k_z}{k} \left(\left| \boldsymbol{\gamma}^+(\boldsymbol{k}_t) \cdot \boldsymbol{F}^+(\boldsymbol{k}_t, z) \right|^2 - \left| \boldsymbol{\gamma}^-(\boldsymbol{k}_t) \cdot \boldsymbol{F}^-(\boldsymbol{k}_t, z) \right|^2 \right) dk_x\, dk_y \end{aligned}$$

Specifically, the power flow of the incident field is

$$P_i = \frac{1}{8\pi^2 \eta\eta_0} \iint_{k_t \le k} \frac{k_z}{k} \left| \boldsymbol{\gamma}^+(\boldsymbol{k}_t) \cdot \boldsymbol{a}_{xy}(\boldsymbol{k}_t) \right|^2 dk_x\, dk_y \tag{2.19}$$

2.4.1 Reflection and transmission dyadics

The relation between the $\boldsymbol{F}^{\pm}$-fields at $z = z_1$ is the well-known reflection dyadic

$$\boldsymbol{F}^-(\boldsymbol{k}_t, z_1) = \mathbf{r}(\boldsymbol{k}_t) \cdot \boldsymbol{F}^+(\boldsymbol{k}_t, z_1) \tag{2.20}$$

Similarly, the relation between the $\boldsymbol{F}^+$-fields evaluated at $z = z_{N-1}$ and $z = z_1$ is the well-known transmission dyadic

$$\boldsymbol{F}^+(\boldsymbol{k}_t, z_{N-1}) = \mathbf{t}(\boldsymbol{k}_t) \cdot \boldsymbol{F}^+(\boldsymbol{k}_t, z_1) \tag{2.21}$$

The reflection and transmission dyadics for the tangential electric field, $\mathbf{r}(\boldsymbol{k}_t)$ and $\mathbf{t}(\boldsymbol{k}_t)$, respectively, are found by the method of propagators. For a stratified, bianisotropic slab the reflection and transmission dyadics are readily found by 4×4 matrix algebra. This technique is presented in detail in [22], and we here present the results of this analysis.

$$\begin{cases} \mathbf{r} = -\mathbf{T}_{22}^{-1} \cdot \mathbf{T}_{21} \\ \mathbf{t} = \mathbf{T}_{11} + \mathbf{T}_{12} \cdot \mathbf{r} \end{cases}$$

where the $\mathbf{T}_{ij}$, $i, j = 1, 2$ are defined as [22]

$$2\mathbf{T}_{ij} = \mathbf{P}_{11} + (-1)^j \mathbf{P}_{12} \cdot \mathbf{O}^{-1} + (-1)^i \mathbf{O} \cdot \mathbf{P}_{12} + (-1)^{i+j} \mathbf{O} \cdot \mathbf{P}_{22} \cdot \mathbf{O}^{-1} \quad i, j = 1, 2$$

and where the propagator dyadics $\mathbf{P}_{ij}$, $i, j = 1, 2$ relates the total fields at $z = z_{N-1}$ and $z = z_1$

$$\begin{pmatrix} \boldsymbol{E}_{xy}(z_{N-1}) \\ \eta\eta_0 \hat{\boldsymbol{z}} \times \boldsymbol{H}_{xy}(z_{N-1}) \end{pmatrix} = \begin{pmatrix} \mathbf{P}_{11} & \mathbf{P}_{12} \\ \mathbf{P}_{21} & \mathbf{P}_{22} \end{pmatrix} \cdot \begin{pmatrix} \boldsymbol{E}_{xy}(z_1) \\ \eta\eta_0 \hat{\boldsymbol{z}} \times \boldsymbol{H}_{xy}(z_1) \end{pmatrix}$$

The propagator dyadics $\mathbf{P}_{ij}$, $i, j = 1, 2$ are readily found for a material that is stratified, *e.g.*, for a homogeneous, isotropic slab we have

$$\begin{pmatrix} \mathbf{P}_{11} & \mathbf{P}_{12} \\ \mathbf{P}_{21} & \mathbf{P}_{22} \end{pmatrix} = e^{ik_0(z_{N-1} - z_1)\mathbf{M}}$$

where

$$\mathbf{M} = \begin{pmatrix} \mathbf{0} & -\mu\mathbf{I}_2 + \frac{1}{\epsilon k_0^2} \boldsymbol{k}_t \boldsymbol{k}_t \\ -\epsilon\mathbf{I}_2 - \frac{1}{\mu k_0^2} \mathbf{J} \cdot \boldsymbol{k}_t \boldsymbol{k}_t \cdot \mathbf{J} & \mathbf{0} \end{pmatrix}$$

From the definition of the wave-spitting, (2.15), and the definition of the reflection dyadic, (2.20), we get

$$\begin{cases} \boldsymbol{E}_{xy}(\boldsymbol{k}_t, z_1) = (\mathbf{I}_2 + \mathbf{r}) \cdot \boldsymbol{F}^+(\boldsymbol{k}_t, z_1) \\ \eta\eta_0 \hat{\boldsymbol{z}} \times \boldsymbol{H}_{xy}(\boldsymbol{k}_t, z_1) = \mathbf{O}^{-1} \cdot (\mathbf{r} - \mathbf{I}_2) \cdot \boldsymbol{F}^+(\boldsymbol{k}_t, z_1) \end{cases} \tag{2.22}$$

The analysis presented so far in this paper is simplified with the use of the following useful relation:

$$\begin{cases} \mathbf{P}^+(\boldsymbol{k}_t) \cdot \mathbf{O}^{-1} + \mathbf{Q}^+(\boldsymbol{k}_t) \cdot \mathbf{J} = \mathbf{0} \\ \mathbf{P}^+(\boldsymbol{k}_t) \cdot \mathbf{O}^{-1} - \mathbf{Q}^+(\boldsymbol{k}_t) \cdot \mathbf{J} = 2\dfrac{k_z}{k}\mathbf{I}_2 - 2\dfrac{k_t}{k}\hat{\boldsymbol{z}}\hat{\boldsymbol{e}}_\parallel = 2\dfrac{k_z}{k}\boldsymbol{\gamma}^+ \\ \mathbf{P}^-(\boldsymbol{k}_t) \cdot \mathbf{O}^{-1} + \mathbf{Q}^-(\boldsymbol{k}_t) \cdot \mathbf{J} = 2\dfrac{k_z}{k}\mathbf{I}_2 + 2\dfrac{k_t}{k}\hat{\boldsymbol{z}}\hat{\boldsymbol{e}}_\parallel = -2\dfrac{k_z}{k}\boldsymbol{\gamma}^- \\ \mathbf{P}^-(\boldsymbol{k}_t) \cdot \mathbf{O}^{-1} - \mathbf{Q}^-(\boldsymbol{k}_t) \cdot \mathbf{J} = \mathbf{0} \end{cases}$$

These equations are readily derived from the definitions of the $\mathbf{P}^\pm$ and $\mathbf{Q}^\pm$ dyadics, (2.7) and (2.8), the definition of the wave-splitting dyadics $\mathbf{O}^{-1}$, (2.16), and the definition of the $\boldsymbol{\gamma}^\pm$ dyadics in (2.6). We have also introduced the dyadic $\mathbf{J} = \hat{\boldsymbol{z}} \times \mathbf{I}_2$, which is a rotation of $\pi/2$ in the x-y-plane. This implies

$$\mathbf{P}^\pm(\boldsymbol{k}_t) \cdot (\mathbf{J} \cdot \eta_0\eta \boldsymbol{H}(\boldsymbol{k}_t, z)) + \mathbf{Q}^\pm(\boldsymbol{k}_t) \cdot (\mathbf{J} \cdot \boldsymbol{E}(\boldsymbol{k}_t, z)) = -2\frac{k_z}{k}\boldsymbol{\gamma}^\pm \cdot \boldsymbol{F}^\pm(\boldsymbol{k}_t, z) \tag{2.23}$$

3 Special case — Flat metallic screen

In this section we specialize the scatterer to a perfectly conducting thin sheet located at $z = z_0$, *i.e.*, $z_< = z_0 = z_>$. The scatterer can be a single scatterer, such as a patch antenna, or many scatterers, *e.g.*, infinite arrays. We get

$$\iint\limits_{S_s} \left(\hat{\boldsymbol{\nu}}(\boldsymbol{r}) \times \boldsymbol{H}(\boldsymbol{r})\right) e^{-i\boldsymbol{k}_t\cdot\boldsymbol{\rho}-ik_z z_0}\, dx\, dy = \boldsymbol{J}_S(\boldsymbol{k}_t) e^{-ik_z z_0}$$

where

$$\boldsymbol{J}_S(\boldsymbol{k}_t) = \iint\limits_{\mathbb{R}^2} \left(\hat{\boldsymbol{z}} \times \left(\boldsymbol{H}^s(\boldsymbol{\rho}, z_0+0) - \boldsymbol{H}^s(\boldsymbol{\rho}, z_0-0)\right)\right) e^{-i\boldsymbol{k}_t\cdot\boldsymbol{\rho}}\, dx\, dy$$

Here $\boldsymbol{J}_S(\boldsymbol{k}_t)$ denotes the sum of Fourier transformed surface currents (exist only on the metallic parts) on the left and right sides of the plane $z = z_0$.

We collect the relevant equations, see (2.10) and (2.14) and use wave-split fields, see (2.22), to replace the fields $\hat{\boldsymbol{z}} \times \boldsymbol{E}(\boldsymbol{k}_t, z_1)$ and $\hat{\boldsymbol{z}} \times \boldsymbol{H}(\boldsymbol{k}_t, z_1)$. We get using (2.23)

$$\begin{cases} \boldsymbol{a}(\boldsymbol{k}_t) = \dfrac{k\eta_0\eta}{2k_z}\mathbf{P}^+(\boldsymbol{k}_t)\cdot\boldsymbol{J}_S(\boldsymbol{k}_t)e^{-ik_z z_0} + \boldsymbol{\gamma}^+\cdot\boldsymbol{F}^+(\boldsymbol{k}_t, z_1)e^{-ik_z z_1} \\ \boldsymbol{\alpha}(\boldsymbol{k}_t) = -\dfrac{k\eta_0\eta}{2k_z}\mathbf{P}^+(\boldsymbol{k}_t)\cdot\boldsymbol{J}_S(\boldsymbol{k}_t)e^{-ik_z z_0} \\ \boldsymbol{\beta}(\boldsymbol{k}_t) = -\boldsymbol{\gamma}^-\cdot\mathbf{r}\cdot\boldsymbol{F}^+(\boldsymbol{k}_t, z_1)e^{ik_z z_1} \end{cases}$$

Especially, the x-y-components are, see (2.6) and (2.7)

$$\begin{cases} \boldsymbol{a}_{xy}(\boldsymbol{k}_t) = \dfrac{k\eta_0\eta}{2k_z}\boldsymbol{\Gamma}(\boldsymbol{k}_t)\cdot\boldsymbol{J}_S(\boldsymbol{k}_t)e^{-ik_z z_0} + \boldsymbol{F}^+(\boldsymbol{k}_t, z_1)e^{-ik_z z_1} \\ \boldsymbol{\alpha}_{xy}(\boldsymbol{k}_t) = -\dfrac{k\eta_0\eta}{2k_z}\boldsymbol{\Gamma}(\boldsymbol{k}_t)\cdot\boldsymbol{J}_S(\boldsymbol{k}_t)e^{-ik_z z_0} \\ \boldsymbol{\beta}_{xy}(\boldsymbol{k}_t) = \mathbf{r}\cdot\boldsymbol{F}^+(\boldsymbol{k}_t, z_1)e^{ik_z z_1} \end{cases} \tag{3.1}$$

The Fourier transform of the transverse scattered electric field in the region $z_0 < z < z_1$ is, see (2.9)

$$\begin{aligned} \boldsymbol{E}^s_{xy}(\boldsymbol{k}_t, z) &= \boldsymbol{\alpha}_{xy}(\boldsymbol{k}_t)e^{ik_z z} + \boldsymbol{\beta}_{xy}(\boldsymbol{k}_t)e^{-ik_z z} \\ &= \boldsymbol{\alpha}_{xy}(\boldsymbol{k}_t)e^{ik_z z} + \mathbf{r}\cdot\boldsymbol{F}^+(\boldsymbol{k}_t, z_1)e^{ik_z(z_1-z)} \\ &= \left(\mathbf{I}_2 e^{ik_z z} + \mathbf{r}e^{ik_z(2z_1-z)}\right)\cdot\boldsymbol{\alpha}_{xy}(\boldsymbol{k}_t) + \mathbf{r}\cdot\boldsymbol{a}_{xy}(\boldsymbol{k}_t)e^{ik_z(2z_1-z)} \end{aligned}$$

This field is evaluated at $z = z_0$. We have

$$\boldsymbol{E}^s_{xy}(\boldsymbol{k}_t, z_0)e^{-ik_z z_0} = \left(\mathbf{I}_2 + \mathbf{r}e^{2ik_z h}\right)\cdot\boldsymbol{\alpha}_{xy}(\boldsymbol{k}_t) + \mathbf{r}\cdot\boldsymbol{a}_{xy}(\boldsymbol{k}_t)e^{2ik_z h}$$

where $h = z_1 - z_0 > 0$. Moreover, we have, see (2.13)

$$\boldsymbol{a}_{xy}(\boldsymbol{k}_t) = \boldsymbol{E}^i_{xy}(\boldsymbol{k}_t, z_0)e^{-ik_z z_0}$$

We therefore get

$$\boldsymbol{E}^s_{xy}(\boldsymbol{k}_t, z_0) = -\frac{k\eta_0\eta}{2k_z}\left(\mathbf{I}_2 + \mathbf{r}e^{2ik_z h}\right)\cdot\boldsymbol{\Gamma}(\boldsymbol{k}_t)\cdot\boldsymbol{J}_S(\boldsymbol{k}_t) + \mathbf{r}\cdot\boldsymbol{E}^i_{xy}(\boldsymbol{k}_t, z_0)e^{2ik_z h} \tag{3.2}$$

We introduce the transverse vector field

$$\boldsymbol{x}(\boldsymbol{k}_t) = \frac{k\eta_0\eta}{2k_z}\boldsymbol{\Gamma}(\boldsymbol{k}_t)\cdot\boldsymbol{J}_S(\boldsymbol{k}_t)$$

and (3.2) is reduced to

$$\boldsymbol{E}^s_{xy}(\boldsymbol{k}_t, z_0) = -\left(\mathbf{I}_2 + \mathbf{r}e^{2ik_z h}\right)\cdot\boldsymbol{x}(\boldsymbol{k}_t) + \mathbf{r}\cdot\boldsymbol{E}^i_{xy}(\boldsymbol{k}_t, z_0)e^{2ik_z h} \tag{3.3}$$

3.1 Transmittance and reflectance

The field at a point $\boldsymbol{r}$ such that $z < z_0$ is given by (2.11)

$$\boldsymbol{E}^s(\boldsymbol{r}) = \frac{1}{4\pi^2}\iint_{-\infty}^{\infty}\boldsymbol{f}(\boldsymbol{k}_t)e^{i\boldsymbol{k}_t\cdot\boldsymbol{\rho}-ik_z z}\,dk_x\,dk_y$$

where, see (2.12), (2.20), and (2.23)

$$\boldsymbol{f}(\boldsymbol{k}_t) = -\frac{k\eta_0\eta}{2k_z}\mathbf{P}^-(\boldsymbol{k}_t)\cdot\boldsymbol{J}_S(\boldsymbol{k}_t)e^{ik_z z_0} - \boldsymbol{\gamma}^-\cdot\mathbf{r}\cdot\boldsymbol{F}^+(\boldsymbol{k}_t, z_1)e^{ik_z z_1}$$

The x-y-components are

$$\boldsymbol{f}_{xy}(\boldsymbol{k}_t) = -\boldsymbol{x}(\boldsymbol{k}_t)e^{ik_z z_0} + \mathbf{r}\cdot\boldsymbol{F}^+(\boldsymbol{k}_t, z_1)e^{ik_z z_1} \tag{3.4}$$

and from (3.1) we get

$$\boldsymbol{f}_{xy}(\boldsymbol{k}_t) = -\boldsymbol{x}(\boldsymbol{k}_t)e^{ik_z z_0} + \mathbf{r}\cdot\left(\boldsymbol{a}_{xy}(\boldsymbol{k}_t) - \boldsymbol{x}(\boldsymbol{k}_t)e^{-ik_z z_0}\right)e^{2ik_z z_1}$$

The power flow of this field is (contains only a $\boldsymbol{F}^-$-part)

$$\begin{aligned}P_r = -\frac{1}{8\pi^2\eta\eta_0}\iint_{k_t\le k}\frac{k_z}{k}\Big|\boldsymbol{\gamma}^-(\boldsymbol{k}_t)\cdot\big(-\boldsymbol{x}(\boldsymbol{k}_t)e^{ik_z z_0}\\ +\mathbf{r}\cdot\left(\boldsymbol{a}_{xy}(\boldsymbol{k}_t) - \boldsymbol{x}(\boldsymbol{k}_t)e^{-ik_z z_0}\right)e^{2ik_z z_1}\big)\Big|^2\,dk_x\,dk_y\end{aligned}$$

The reflected power divided by the incident power, P_i, see (2.19), is the reflectance R, *i.e.*,

$$R = \frac{P_r}{P_i}$$

The transmitted field $z > z_{N-1}$ is determined by, see (2.21)

$$\boldsymbol{F}^+(\boldsymbol{k}_t, z_{N-1}) = \mathbf{t}(\boldsymbol{k}_t)\cdot\boldsymbol{F}^+(\boldsymbol{k}_t, z_1)$$

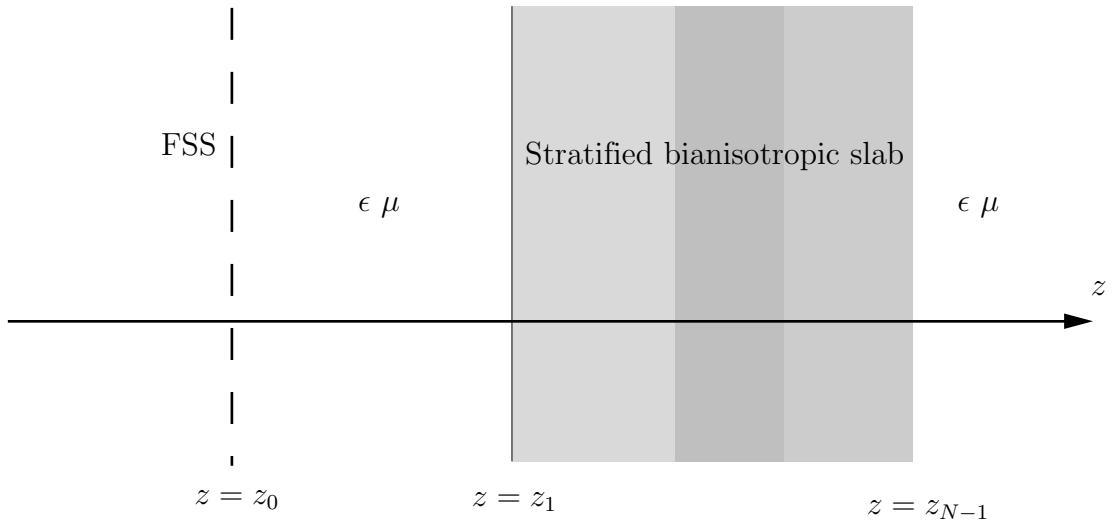

Figure 2: The geometry of the FSS and the slab.

Use (3.1) and we get

$$\boldsymbol{F}^+(\boldsymbol{k}_t, z_{N-1}) = \mathbf{t}(\boldsymbol{k}_t) \cdot \left(\boldsymbol{a}_{xy}(\boldsymbol{k}_t) e^{ik_z z_1} - \boldsymbol{x}(\boldsymbol{k}_t) e^{ik_z h}\right)$$

The power flow of this field is

$$P_t = \frac{1}{8\pi^2 \eta \eta_0} \iint\limits_{k_t \le k} \frac{k_z}{k} \left| \boldsymbol{\gamma}^+(\boldsymbol{k}_t) \cdot \mathbf{t}(\boldsymbol{k}_t) \cdot \left(\boldsymbol{a}_{xy}(\boldsymbol{k}_t) e^{ik_z z_1} - \boldsymbol{x}(\boldsymbol{k}_t) e^{ik_z h}\right) \right|^2 dk_x\, dk_y$$

The transmitted power divided by the incident power, P_i, see (2.19), is the transmittance T, *i.e.*,

$$T = \frac{P_t}{P_i}$$

4 Special case — FSS

In the previous sections, we started with a general formulation where the scatterer enclosed inside the surface S_s was a general body (metallic or permeable). This assumption was relaxed in Section 3 where we specialized the scatterer to a thin metallic sheet. We now restrict our scatterer further, so that in addition to being flat, we also assume it to be periodic in the plane $z = z_0$, see Figure 2. Moreover, in this section we treat only the patch case — the corresponding aperture case is treated by the duality principle [18].

In this section, we assume the incident wave to be a plane wave, *i.e.*,

$$\boldsymbol{E}^i(\boldsymbol{r}) = \boldsymbol{E}_0^i e^{i\boldsymbol{k}^i \cdot \boldsymbol{r}}$$

where $\boldsymbol{k}^i$ is the wave vector of the incident wave, and $\boldsymbol{E}_0^i$ is a constant complex vector such that $\boldsymbol{E}_0^i \cdot \boldsymbol{k}^i = 0$. The Fourier transform of this field evaluated at $z =$ constant

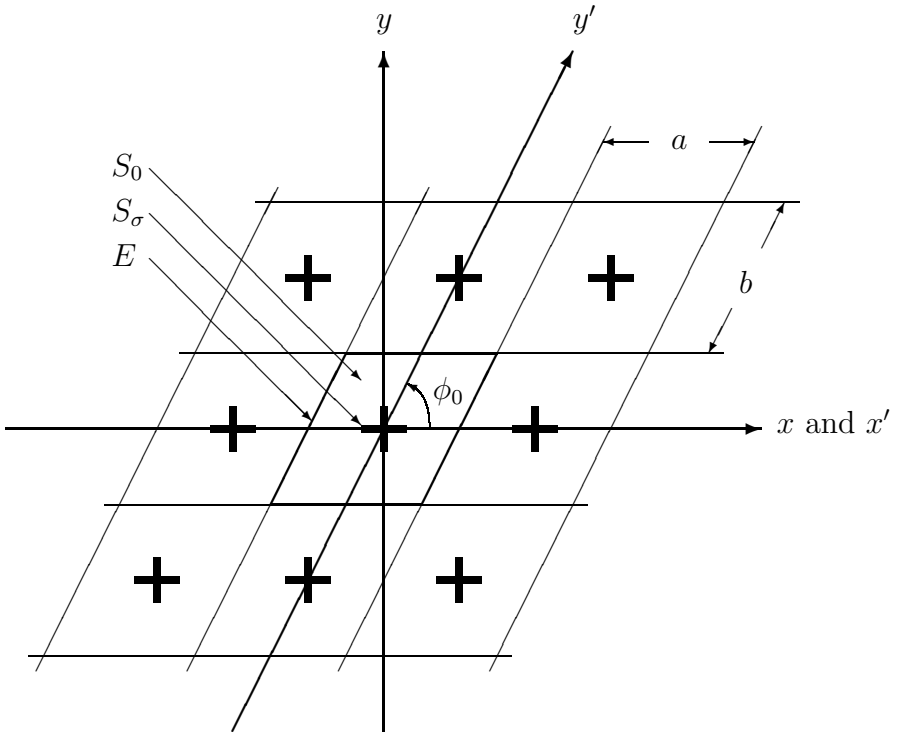

Figure 3: The unit cell E with the sides a and b.

is

$$\boldsymbol{a}_{xy}(\boldsymbol{k}_t)e^{ik_z z} = \boldsymbol{E}^i(\boldsymbol{k}_t, z) = 4\pi^2 \boldsymbol{E}_0^i e^{ik_z^i z}\delta^2(\boldsymbol{k}_t - \boldsymbol{k}_t^i)$$

where $k_z^i = \boldsymbol{k}^i \cdot \hat{\boldsymbol{z}}$ and $\boldsymbol{k}_t^i = \mathbf{I}_2 \cdot \boldsymbol{k}^i$. The spherical angles of $\boldsymbol{k}^i$ are denoted θ (polar angle) and ϕ (azimuth angle) and the components of $\boldsymbol{k}^i$ in the x-y-plane are denoted by k_x^i and k_y^i, respectively.

The periodicity of the scatterer (FSS) in the x-y-plane is a and b, respectively, see Figure 3. The periodic pattern can be obliquely oriented and ϕ_0 denotes the angle between the axes of periodicity. We denote the unit cell by E (area A_E), and the metallic parts in the unit cell by S_σ.

4.1 Integral equation for the surface current

We employ the Floquet's theorem [8] to the surface current $\boldsymbol{J}_S$ and the result is [20]

$$\boldsymbol{J}_S(\boldsymbol{\rho}) = \hat{\boldsymbol{z}} \times (\boldsymbol{H}^s(\boldsymbol{\rho}, z_0 + 0) - \boldsymbol{H}^s(\boldsymbol{\rho}, z_0 - 0)) = \frac{1}{A_E} \sum_{m,n=-\infty}^{\infty} \boldsymbol{J}_E(\boldsymbol{k}_{mn}) e^{i\boldsymbol{k}_{mn}\cdot\boldsymbol{\rho}}$$

where $\boldsymbol{\rho} \in \mathbb{R}^2$, and $\boldsymbol{k}_{mn} = \hat{\boldsymbol{x}}\alpha_m + \hat{\boldsymbol{y}}\beta_{mn}$ with

$$\begin{cases} \alpha_m = \dfrac{2\pi m}{a} + k_x^i \\ \beta_{mn} = \dfrac{2\pi n}{b\sin\phi_0} - \dfrac{2\pi m}{a}\cot\phi_0 + k_y^i \end{cases}$$

and where $\boldsymbol{J}_E(\boldsymbol{k}_{mn})$ is the Fourier transform of $\boldsymbol{J}_S(\boldsymbol{\rho})$ over the unit cell E evaluated at $\boldsymbol{k}_{mn}$. The Fourier transform of the current is

$$\boldsymbol{J}_S(\boldsymbol{k}_t) = \frac{4\pi^2}{A_E} \sum_{m,n=-\infty}^{\infty} \boldsymbol{J}_E(\boldsymbol{k}_{mn}) \delta^2(\boldsymbol{k}_t - \boldsymbol{k}_{mn}), \quad \boldsymbol{k}_t \in \mathbb{R}^2 \tag{4.1}$$

Insert (4.1) into (3.3) and take an inverse Fourier transform. The result is

$$\begin{aligned} \boldsymbol{E}^s_{xy}(\boldsymbol{r})\big|_{z=z_0} = &- \sum_{m,n=-\infty}^{\infty} \left(\mathbf{I}_2 + \mathbf{r}(\boldsymbol{k}_{mn}) e^{2ik_{zmn}h}\right) \cdot \boldsymbol{x}_{mn} e^{i\boldsymbol{k}_{mn}\cdot\boldsymbol{\rho}} \\ &+ \mathbf{r}(\boldsymbol{k}_{00}) e^{2ik_{z00}h} \cdot \boldsymbol{E}^i_{xy}(\boldsymbol{r})\big|_{z=z_0} \end{aligned} \tag{4.2}$$

where

$$k_{zmn} = \begin{cases} \sqrt{k^2 - |\boldsymbol{k}_{mn}|^2} \text{ for } |\boldsymbol{k}_{mn}| < k \\ i\sqrt{|\boldsymbol{k}_{mn}|^2 - k^2} \text{ for } |\boldsymbol{k}_{mn}| > k \end{cases}$$

and where we have introduced the vector field

$$\boldsymbol{x}_{mn} = \frac{k\eta_0\eta}{2A_E k_{zmn}} \boldsymbol{\Gamma}(\boldsymbol{k}_{mn}) \cdot \boldsymbol{J}_E(\boldsymbol{k}_{mn})$$

to simplify the notation.

For a $\boldsymbol{\rho}$ on S_σ we get from (4.2)

$$\left(\mathbf{I}_2 + \mathbf{r}(\boldsymbol{k}_{00}) e^{2ik_{z00}h}\right) \cdot \boldsymbol{E}^i_{xy}(\boldsymbol{r})\big|_{z=z_0} = \sum_{m,n=-\infty}^{\infty} \left(\mathbf{I}_2 + \mathbf{r}(\boldsymbol{k}_{mn}) e^{2ik_{zmn}h}\right) \cdot \boldsymbol{x}_{mn} e^{i\boldsymbol{k}_{mn}\cdot\boldsymbol{\rho}} \tag{4.3}$$

This relation is the basic equation used for the determination of the unknown quantity $\boldsymbol{x}_{mn}$. Once this quantity is determined, all other fields can be obtained.

4.2 Galerkin's procedure

The current in the unit cell, $\boldsymbol{J}_E(\boldsymbol{\rho})$, can be expanded with arbitrary precision in a pertinent complete set of entire domain basis functions $\boldsymbol{j}_p(\boldsymbol{\rho})$, *i.e.*,

$$\boldsymbol{J}_E(\boldsymbol{\rho}) = \sum_{p\in\chi} C_p \boldsymbol{j}_p(\boldsymbol{\rho}) \tag{4.4}$$

where χ is a set of indices (countable set) and the scalars C_p are the unknown expansion coefficients. We also have from (4.4) by taking the Fourier transform

$$\boldsymbol{x}_{mn} = \sum_{p\in\chi} C_p \boldsymbol{x}_{mn,p} \tag{4.5}$$

where

$$\boldsymbol{x}_{mn,p} = \frac{k\eta_0\eta}{2A_E k_{zmn}} \boldsymbol{\Gamma}(\boldsymbol{k}_{mn}) \cdot \boldsymbol{j}_p(\boldsymbol{k}_{mn})$$

We make a scalar multiplication of (4.3) with $\boldsymbol{j}_q^*(\boldsymbol{\rho})$, where * denotes the complex conjugate, and integrate over the conducting part of the unit cell, S_σ. Then, the left and right hand side can be identified as a Fourier transform, *i.e.*,

$$\begin{aligned}\boldsymbol{j}_q^*(\boldsymbol{k}_{00})\cdot \left(\mathbf{I}_2 + \mathbf{r}(\boldsymbol{k}_{00})e^{2ik_{z00}h}\right)\cdot \boldsymbol{E}^i_{xy}e^{ik^i_z z_0}& \\ = \sum_{m,n=-\infty}^{\infty} \boldsymbol{j}_q^*(\boldsymbol{k}_{mn})\cdot \left(\mathbf{I}_2 + \mathbf{r}(\boldsymbol{k}_{mn})e^{2ik_{z\,mn}h}\right)\cdot \boldsymbol{x}_{mn} & \quad q\in\chi\end{aligned}$$

Finally, we replace the unit cell current with its basis function expansion (4.5). We have

$$\begin{aligned}\boldsymbol{j}_q^*(\boldsymbol{k}_{00})\cdot \left(\mathbf{I}_2 + \mathbf{r}(\boldsymbol{k}_{00})e^{2ik_{z00}h}\right)\cdot \boldsymbol{E}^i_{xy}e^{ik^i_z z_0}& \\ = \sum_{m,n=-\infty}^{\infty}\sum_{p\in\chi} C_p\boldsymbol{j}_q^*(\boldsymbol{k}_{mn})\cdot \left(\mathbf{I}_2 + \mathbf{r}(\boldsymbol{k}_{mn})e^{2ik_{z\,mn}h}\right)\cdot \boldsymbol{x}_{mn,p} & \quad q\in\chi\end{aligned}$$

If χ is an infinite set of indices, the above equation is an infinite system of linear equations for the unknown current coefficients C_p. We assume that if this infinite system is truncated, the solution to the truncated system approximates the exact solution. When the linear system is truncated, it can be written

$$\mathbf{A}\boldsymbol{C} = \boldsymbol{b}$$

where $\mathbf{A}$ is a square matrix, $\boldsymbol{C}$ is a vector containing the unknown coefficients C_p, and $\boldsymbol{b}$ is a known vector.

4.3 The reflection and transmission coefficients

We assume that the solution of (4.3), $\boldsymbol{x}_{mn}$, is known, *e.g.*, it is obtained by the Galerkin method presented in Section 4.2. Therefore, the current $\boldsymbol{J}_E(\boldsymbol{\rho})$ is known or even more appropriate its Fourier transform $\boldsymbol{J}_E(\boldsymbol{k}_{mn})$. The relation to the Fourier transform of the current $\boldsymbol{J}_S(\boldsymbol{k}_t)$ is, (4.1)

$$\boldsymbol{x}(\boldsymbol{k}_t) = 4\pi^2\sum_{m,n=-\infty}^{\infty}\boldsymbol{x}_{mn}\delta^2(\boldsymbol{k}_t - \boldsymbol{k}_{mn}),\quad \boldsymbol{k}_t\in\mathbb{R}^2$$

The field at a point $\boldsymbol{r}$ such that $z < z_<$ is given by (2.11) as

$$\boldsymbol{E}^s(\boldsymbol{r}) = \frac{1}{4\pi^2}\iint_{-\infty}^{\infty}\boldsymbol{f}(\boldsymbol{k}_t)e^{i\boldsymbol{k}_t\cdot\boldsymbol{\rho}-ik_z z}\,dk_x\,dk_y$$

where, see (3.4),

$$\boldsymbol{f}(\boldsymbol{k}_t) = -\frac{k\eta_0\eta}{2k_z}\mathbf{P}^-(\boldsymbol{k}_t)\cdot\boldsymbol{J}_S(\boldsymbol{k}_t)e^{ik_z z_0} - \boldsymbol{\gamma}^-\cdot\mathbf{r}\cdot\boldsymbol{F}^+(\boldsymbol{k}_t, z_1)e^{ik_z z_1}$$

Moreover, from (3.1) we get

$$\boldsymbol{F}^{+}(\boldsymbol{k}_t, z_1) = e^{ik_z z_1}\left(\boldsymbol{a}_{xy}(\boldsymbol{k}_t) - \frac{k\eta_0\eta}{2k_z}\boldsymbol{\Gamma}(\boldsymbol{k}_t)\cdot\boldsymbol{J}_S(\boldsymbol{k}_t)e^{-ik_z z_0}\right)$$

and thus, $\boldsymbol{f}(\boldsymbol{k}_t)$ is simplified to

$$\begin{aligned}\boldsymbol{f}(\boldsymbol{k}_t) = \frac{k\eta_0\eta}{2k_z}e^{ik_z z_0}\left\{e^{2ik_z(z_1-z_0)}\boldsymbol{\gamma}^{-}\cdot\mathbf{r}\cdot\boldsymbol{\Gamma}(\boldsymbol{k}_t) - \mathbf{P}^{-}(\boldsymbol{k}_t)\right\}\cdot\boldsymbol{J}_S(\boldsymbol{k}_t)\\ - e^{ik_z(z_1+z_0)}\boldsymbol{\gamma}^{-}\cdot\mathbf{r}\cdot\boldsymbol{a}_{xy}(\boldsymbol{k}_t)\end{aligned}$$

We introduce the wave vector of the transmitted and reflected field as $\boldsymbol{k}_{mn}^{\pm} = \boldsymbol{k}_{mn} \pm \hat{z}k_{zmn}$. Then, from (4.1) we obtain

$$\boldsymbol{E}^{s}(\boldsymbol{r}) = \left(\mathbf{S}^{-}\cdot\boldsymbol{E}_{xy}^{i}\right)e^{i\boldsymbol{k}_{00}^{-}\cdot\boldsymbol{r}} + \sum_{m,n=-\infty}^{\infty}\mathbf{G}_{mn}^{-}\cdot\boldsymbol{J}_E(\boldsymbol{k}_{mn})e^{i\boldsymbol{k}_{mn}^{-}\cdot\boldsymbol{r}} \quad z < z_{<}$$

where

$$\begin{cases}\mathbf{G}_{mn}^{-} = \dfrac{k\eta_0\eta}{2A_E k_{zmn}}e^{ik_{zmn}z_0}\left[e^{2ik_{zmn}h}\boldsymbol{\gamma}_{mn}^{-}\cdot\mathbf{r}_{mn}\cdot\boldsymbol{\Gamma}_{mn} - \mathbf{P}_{mn}^{-}\right]\\ \mathbf{S}^{-} = -e^{ik_{z00}(h+2z_0)}\boldsymbol{\gamma}_{00}^{-}\cdot\mathbf{r}_{00}\end{cases}$$

where, as before, $h = z_1 - z_0$. We have also introduced the notation $\boldsymbol{\gamma}_{mn} = \boldsymbol{\gamma}(\boldsymbol{k}_{mn})$ and similarly for the other quantities with indices mn.

In the absence of the slab, *i.e.*, $\mathbf{r} = \mathbf{0}$, and with the FSS located at $z_0 = 0$, we have

$$\begin{cases}\mathbf{G}_{mn}^{-} = -\dfrac{k\eta_0\eta}{2A_E k_{zmn}}\mathbf{P}^{-}(\boldsymbol{k}_{mn})\\ \mathbf{S}^{-} = \mathbf{0}\end{cases}\qquad \text{no slab}$$

In order to identify the reflection dyadic of the FSS and the substrate, we introduce the dyadic $\mathbf{C}_{mn}^{-}$ implicitly defined by

$$\mathbf{C}_{mn}^{-}\cdot\boldsymbol{E}_{xy}^{i} = \mathbf{G}_{mn}^{-}\cdot\boldsymbol{J}_E(\boldsymbol{k}_{mn})$$

This definition enables us to define the reflection dyadic $\mathbf{R}_{mn}$ of the FSS and the slab as

$$\mathbf{R}_{mn} = \mathbf{S}^{-}\delta_{m,0}\delta_{n,0} + \mathbf{C}_{mn}^{-}$$

The co- and cross-polarized components of the reflection dyadic are

$$\hat{\boldsymbol{e}}_i(\boldsymbol{k}_{mn})\cdot\mathbf{R}_{mn}\cdot\hat{\boldsymbol{e}}_j(\boldsymbol{k}_{mn})$$

The $i = 1$ ($i = 2$) and $j = 1$ ($j = 2$) are the co-polarized TM (TE) contributions. The off diagonal parts give the cross-polarizations. The fundamental mode corresponds to $m = n = 0$.

Only the homogeneous part of the field ($k_t < k$) contributes to the far field. If $k_{mn} > k$ for all $(m, n) \neq (0, 0)$, we have no grating lobes. This is the case of most

technical interest. Assuming this is the case, we have the reflectance R of the FSS defined as

$$R = \lim_{z\to-\infty} \frac{\left|\boldsymbol{E}^s(\boldsymbol{r})\right|^2}{\left|\boldsymbol{E}_0^i\right|^2}$$
$$= \frac{\left|\mathbf{S}^- \cdot \boldsymbol{E}_{xy}^i + \mathbf{G}_{00}^- \cdot \boldsymbol{J}_E(\boldsymbol{k}_{00})\right|^2}{\left|\boldsymbol{E}_0^i\right|^2} = \frac{\left|\mathbf{R}_{00} \cdot \boldsymbol{E}_{xy}^i\right|^2}{\left|\boldsymbol{E}_0^i\right|^2}, \qquad \text{no grating lobes}$$

We now proceed and calculate the transmitted field. On the right side of the slab, $z > z_{N-1}$, the fields only propagate in the positive z-direction, thus $\boldsymbol{F}^+(\boldsymbol{k}_t, z) = \boldsymbol{E}_{xy}^t(\boldsymbol{k}_t, z)$. We obtain the relation between $\boldsymbol{F}^+(\boldsymbol{k}_t, z_{N-1})$ and $\boldsymbol{F}^+(\boldsymbol{k}_t, z_1)$ in terms of the transmission dyadic $\mathbf{t}(\boldsymbol{k}_t)$ from (2.21).

$$\boldsymbol{F}^+(\boldsymbol{k}_t, z_{N-1}) = \mathbf{t}(\boldsymbol{k}_t) \cdot \boldsymbol{F}^+(\boldsymbol{k}_t, z_1)$$

The field $\boldsymbol{F}^+(\boldsymbol{k}_t, z_1)$ is derived from the quantity $\boldsymbol{x}_{mn}$ and are therefore assumed known, see (3.1), *i.e.*,

$$\boldsymbol{F}^+(\boldsymbol{k}_t, z_1) = \boldsymbol{a}_{xy}(\boldsymbol{k}_t) e^{ik_z z_1} - \frac{k\eta_0\eta}{2k_z} \boldsymbol{\Gamma}(\boldsymbol{k}_t) \cdot \boldsymbol{J}_S(\boldsymbol{k}_t) e^{ik_z h}$$

All three components of the field (including the z-component) is obtained from the field $\boldsymbol{E}_{xy}^t$ by a multiplication by the dyadic $\boldsymbol{\gamma}^+(\boldsymbol{k}_t)$. Take the inverse Fourier transform and we obtain the transmitted field in the region $z > z_{N-1}$

$$\boldsymbol{E}^t(\boldsymbol{r}) = \frac{1}{4\pi^2} \iint \boldsymbol{\gamma}^+(\boldsymbol{k}_t) \cdot \boldsymbol{F}^+(\boldsymbol{k}_t, z_{N-1}) e^{i\boldsymbol{k}_t \cdot \boldsymbol{\rho}} e^{ik_z(z - z_{N-1})} dk_x dk_y$$

Finally, (4.1) gives the final expression

$$\boldsymbol{E}^t(\boldsymbol{r}) = \left(\mathbf{S}^+ \cdot \boldsymbol{E}_{xy}^i\right) e^{i\boldsymbol{k}_{00}^+ \cdot \boldsymbol{r}} + \sum_{m,n=-\infty}^{\infty} \mathbf{G}_{mn}^+ \cdot \boldsymbol{J}_E(\boldsymbol{k}_{mn}) e^{\boldsymbol{k}_{mn}^+ \cdot \boldsymbol{r}}$$

where

$$\begin{cases} \mathbf{G}_{mn}^+ = -\dfrac{k\eta_0\eta}{2A_E k_{z_{mn}}} e^{ik_{z_{mn}}(h - z_{N-1})} \boldsymbol{\gamma}_{mn}^+ \cdot \mathbf{t}_{mn} \cdot \boldsymbol{\Gamma}_{mn} \\ \mathbf{S}^+ = e^{ik_{z00}(h - 2z_0 - z_{N-1})} \boldsymbol{\gamma}_{00}^+ \cdot \mathbf{t}_{00} \end{cases}$$

Analogous to the reflection dyadic defined above, we introduce the transmission dyadic of the FSS and the substrate. To this end, the dyadic $\mathbf{C}_{mn}^+$ is implicitly defined by

$$\mathbf{C}_{mn}^+ \cdot \boldsymbol{E}_{xy}^i = \mathbf{G}_{mn}^+ \cdot \boldsymbol{J}_E(\boldsymbol{k}_{mn})$$

This definition enables us to define the transmission dyadic $\mathbf{T}_{mn}$ of the FSS and the slab as

$$\mathbf{T}_{mn} = \mathbf{S}^+ \delta_{m,0} \delta_{n,0} + \mathbf{C}_{mn}^+$$

The co- and cross-polarized components of the transmission dyadic are

$$\hat{\boldsymbol{e}}_i(\boldsymbol{k}_{mn}) \cdot \mathbf{T}_{mn} \cdot \hat{\boldsymbol{e}}_j(\boldsymbol{k}_{mn})$$

The $i = 1$ ($i = 2$) and $j = 1$ ($j = 2$) are the co-polarized TM (TE) contributions. The off diagonal parts give the cross-polarizations. The fundamental mode corresponds to $m = n = 0$.

As before, only the homogeneous part of the field ($k_t < k$) contributes to the far field. In the absence of grating lobes, we have the transmittance T of the FSS defined as

$$T = \lim_{z\to\infty} \frac{\left|\boldsymbol{E}^t(\boldsymbol{r})\right|^2}{\left|\boldsymbol{E}_0^i\right|^2} = \frac{\left|\mathbf{S}^+ \cdot \boldsymbol{E}_{xy}^i + \mathbf{G}_{00}^+ \cdot \boldsymbol{J}_E(\boldsymbol{k}_{00})\right|^2}{\left|\boldsymbol{E}_0^i\right|^2} = \frac{\left|\mathbf{T}_{00} \cdot \boldsymbol{E}_{xy}^i\right|^2}{\left|\boldsymbol{E}_0^i\right|^2}, \qquad \text{no grating lobes}$$

5 Results

We illustrate the theory presented in this paper by a series of numerical computations for a set of standard element patterns and a multitude of slabs. In some cases the computations are compared with experimental measurements. These computations are not meant to be good candidates for a FSS design, but merely an illustration of what we can accomplish with the method.

As a first example, we illustrate the effect of an isotropic, homogeneous dielectric substrate on the transmission properties of the FSS in Figure 4. The geometry of the elements and periodicity are given in the captions and in Figure 5. The broken line shows the numerical computations and the solid line shows the measured results. A similar case for oblique incidence is given in Figure 6.

In a multitude of applications, the substrate is reinforced by a glass fiber layer for mechanical reasons. The glass fiber introduces an uniaxial effect that in most practical situations can be modelled by a homogenized layer, see *e.g.*, Ref. 21. To illustrate the effect of the presence of a uniaxial substrate, we compute the resonance frequency for a series of different values of the permittivity of the substrate. The shift in the resonance frequency is depicted in Figure 7. We observe that the shift in the resonance frequency due to the anisotropy is small for small anisotropies, but larger for a larger value on the permittivity. We also note that the transverse components of the permittivity dyadic effect the resonance frequency more than the z-component.

The effect of a bianisotropic substrate is illustrated in Figure 8. The constitutive relations used here are [22]

$$\begin{cases} \boldsymbol{D} = \epsilon_0 \left\{ \boldsymbol{\epsilon} \cdot \boldsymbol{E} + \eta_0 \boldsymbol{\xi} \cdot \boldsymbol{H} \right\} \\ \boldsymbol{B} = \dfrac{1}{c_0} \left\{ \boldsymbol{\zeta} \cdot \boldsymbol{E} + \eta_0 \boldsymbol{\mu} \cdot \boldsymbol{H} \right\} \end{cases}$$

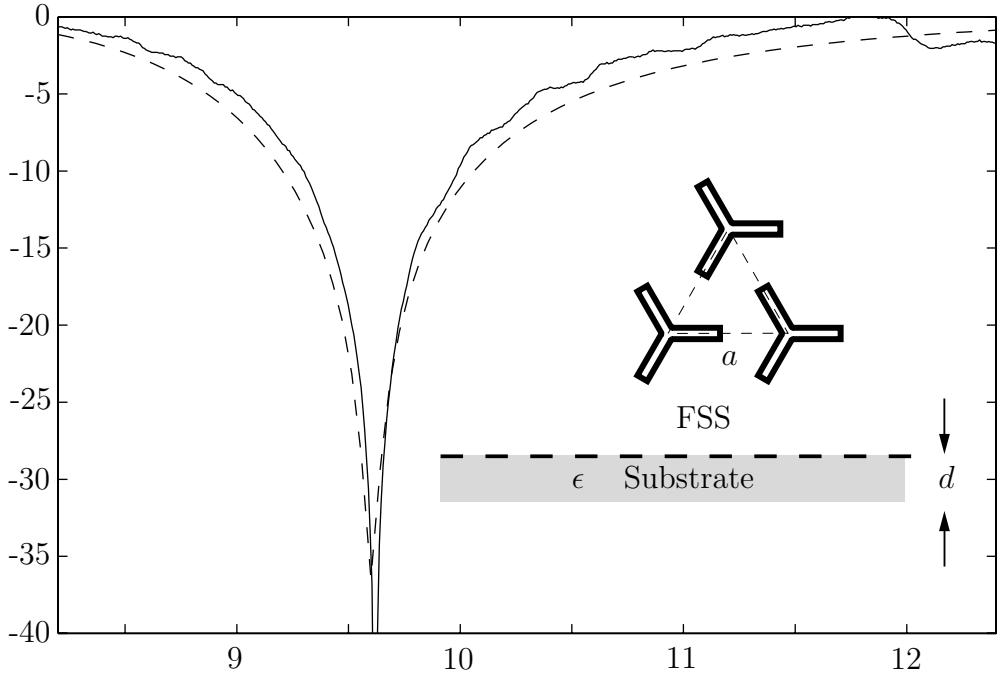

Figure 4: Power transmission (in dB scale) at normal incidence of the co-polarization at 8.2–12.4 GHz for a hexagonal pattern of loaded tripoles on an isotropic slab. The tripoles are 9 mm long with 3 mm long ends, see Figure 5. The width of the metallic strips is 0.5 mm. The elements are arranged in an equilateral lattice with side $a = b = 16.5$ mm. The polarization of the incident field is perpendicular with one of the sides in the hexagonal pattern. The thickness of the isotropic substrate is $d = 0.12$ mm and the permittivity is $\epsilon = 4.3(1 + i0.021)$. The broken line shows the numerical computations and the solid line shows the measured results.

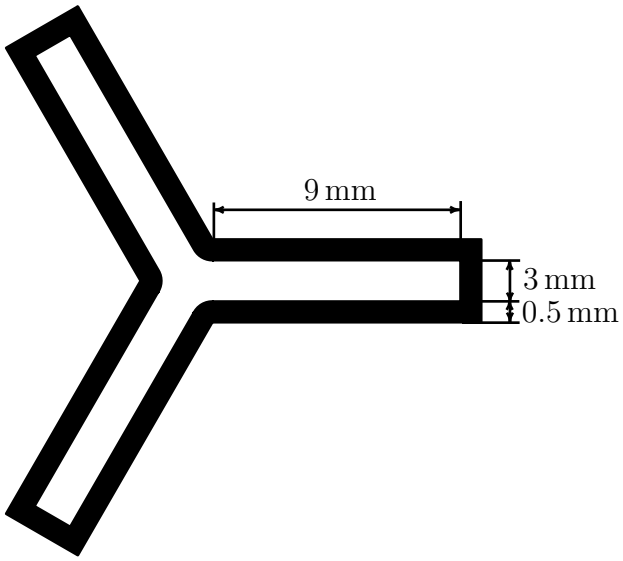

Figure 5: The geometry of the loaded tripoles.

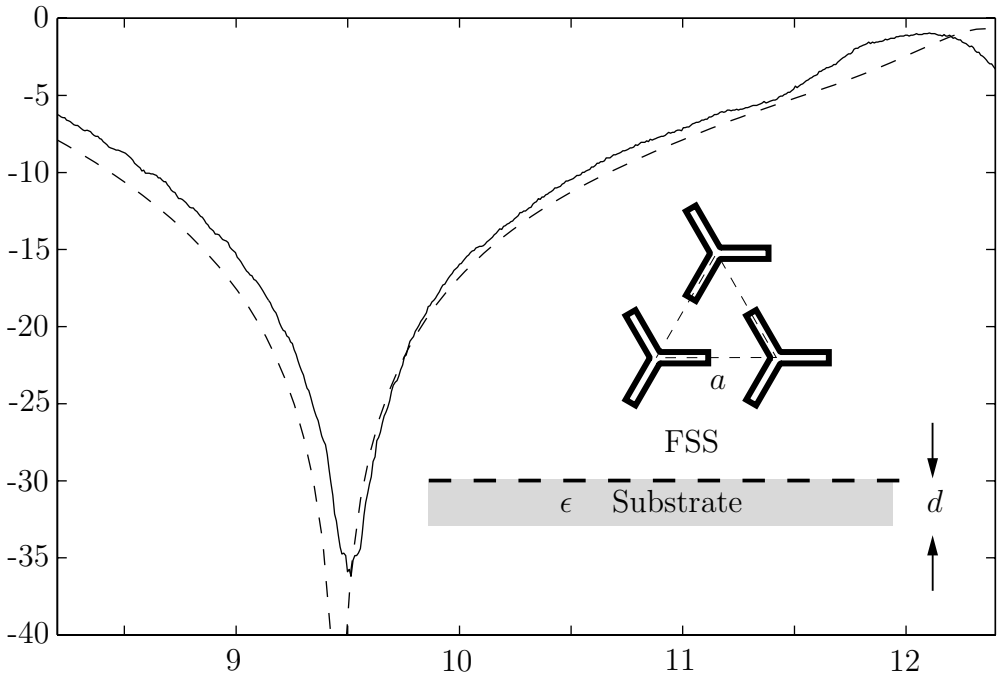

Figure 6: Power transmission (in dB scale) of the co-polarization at 8.2–12.4 GHz for a hexagonal pattern of loaded tripoles on an isotropic slab. The geometry is same as in Figure 4, but the angle of incidence is $\theta = 60°$ and $\phi = 0°$, and the polarization is TE. The broken line shows the numerical computations and the solid line shows the measured results.

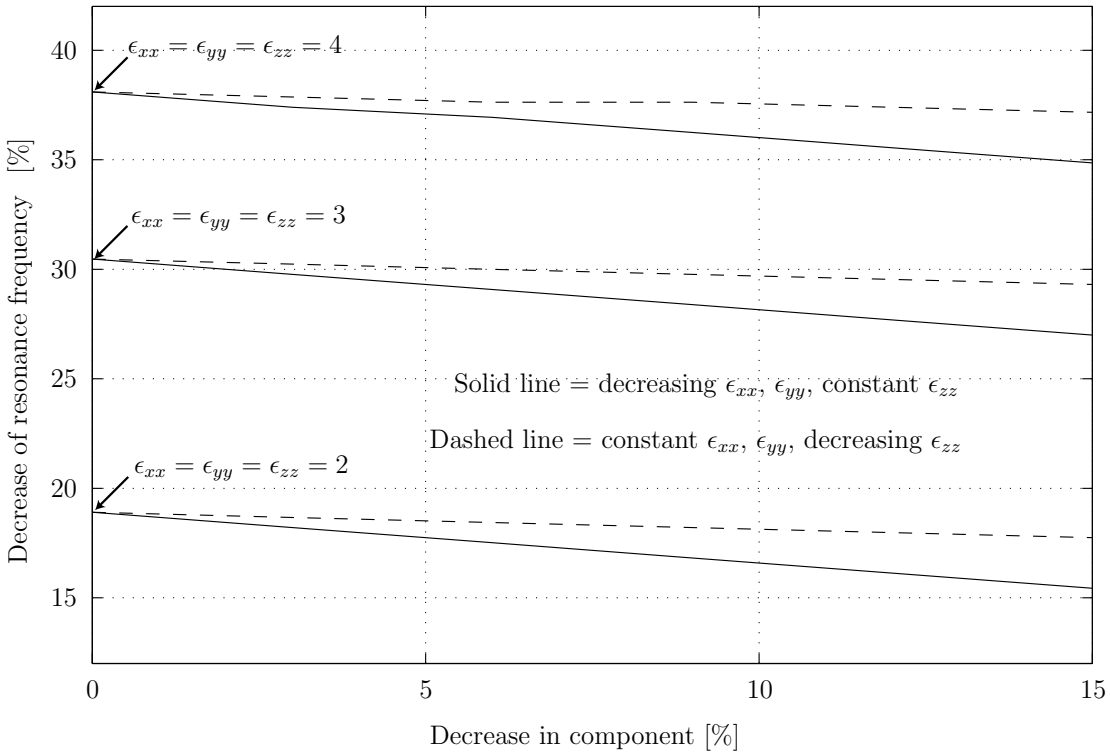

Figure 7: The relative change in the resonance frequency for crossed dipoles versus the degree of relative anisotropy of the slab relative an FSS without substrate. The left side of the graph corresponds to the shift in the resonance frequency due to the presence of an isotropic substrate. The thickness of the substrate is $d = 5$ mm. The arms of the dipoles are 9 mm long and 1 mm wide, and the crossed dipoles are arranged in a oblique pattern tilted $\phi_0 = 45^\circ$ with $a = 14.1$ mm and $b = 10$ mm. The angle of incidence is $\theta = 0^\circ$ and $\phi = 45^\circ$.

The material parameters of the slab is [19]

$$\boldsymbol{\epsilon} = \begin{pmatrix} 3 & 0 & 0 \\ 0 & \epsilon_{yy} & 0 \\ 0 & 0 & 3 \end{pmatrix} \quad \boldsymbol{\mu} = \begin{pmatrix} 1 & 0 & 0 \\ 0 & 1 & 0 \\ 0 & 0 & 1 \end{pmatrix} \quad \boldsymbol{\xi} = \begin{pmatrix} 0 & 0 & 0 \\ 0 & 0 & i\Omega \\ 0 & 0 & 0 \end{pmatrix} \quad \boldsymbol{\zeta} = \begin{pmatrix} 0 & 0 & 0 \\ 0 & 0 & 0 \\ 0 & -i\Omega & 0 \end{pmatrix} \tag{5.1}$$

6 Conclusion and discussion

In this paper we present a new method to compute the reflection and transmission properties of FSSs supported by bianisotropic substrates. The elements of the FSS are arbitrary, and the substrate, located on one side of the FSS, consists of an arbitrary bianisotropic material, which is stratified (piecewise constant parameters) or has continuously varying parameters with respect to depth. The method presented in this paper relies on a systematic use of the integral representation of the elec-

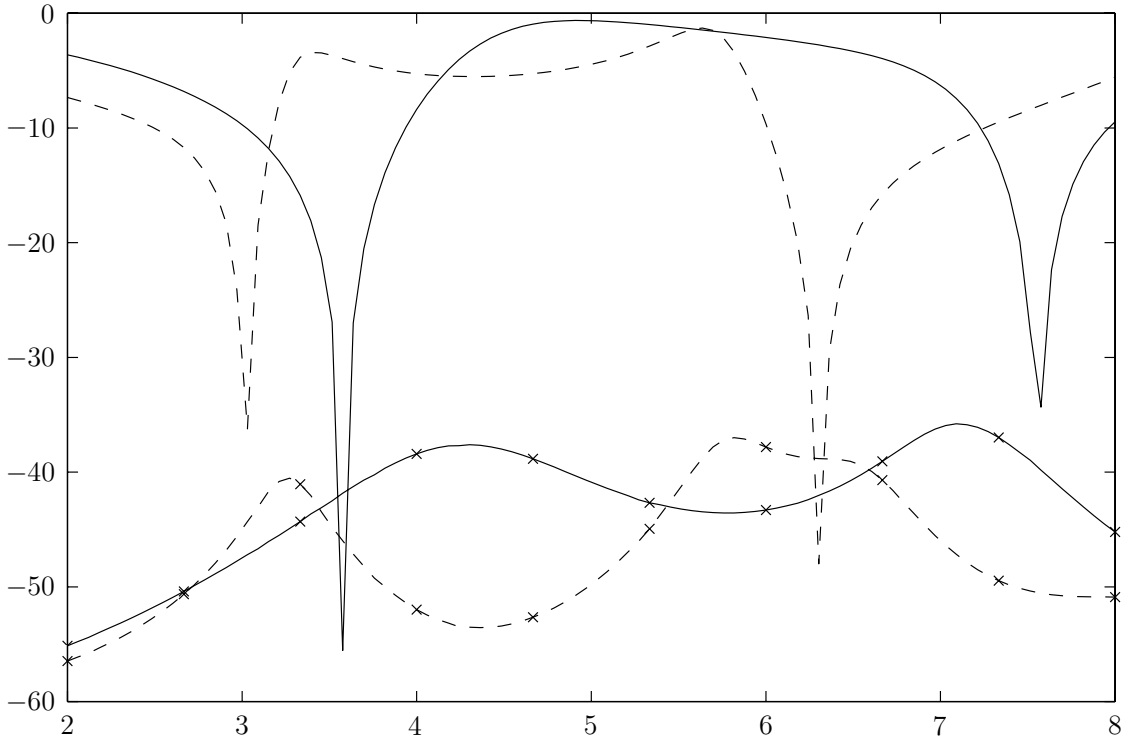

Figure 8: The same element and unit cell geometry as in Figures 4 and 6 but the substrate is bianisotropic and the frequency range is larger. The material parameters is given in (5.1) and the thickness of the substrate is $d = 6$ mm. The curves that correspond to the co-polarization are given by lines without crosses and the cross-polarization curves are given by lines with crosses. The solid lines show the cases where $\epsilon_{yy} = 3$ and $\Omega = 0$ (*i.e.*, an isotropic substrate), and the dashed lines show the cases where $\epsilon_{yy} = 10$ and $\Omega = 0.9$. The angle of incidence is $\theta = 30^\circ$ and $\phi = 0^\circ$, and the polarization is TE.

tromagnetic fields outside the slab. The unknown current on the FSS is obtained by an application of the method of moments, and from its solution all other quantities are calculated. In a series of numerical computations the performance of the method is illustrated. These illustrations are not intended to be candidates for an actual design, but merely an illustration of the performance of the method and its potential.

The method applies to a slab located on one side of the FSS, but with appropriate generalizations it will apply to the situation where we have a bianisotropic slab on each side of the FSS, as well as the situation of multi-layered FSSs. These generalizations will be addressed in a subsequent paper.

Acknowledgements

The work reported in this paper is supported by grants from the Swedish Defence Materiel Administration (FMV) and by the Swedish Foundation for Strategic Research (SSF), which are gratefully acknowledged.

Appendix A Power flow

The average power in the z-direction is determined by the integral of Poynting's vector over a plane $z =$ constant. Provided the material parameters are constant on the plane $z =$ constant, we have a Fourier representation of the fields. Using the Parseval's identity, we get

$$\begin{aligned}\iint_{-\infty}^{\infty} \hat{\boldsymbol{z}} \cdot \boldsymbol{S}(\boldsymbol{r})\, dx\, dy &= \frac{1}{2}\,\mathrm{Re} \iint_{-\infty}^{\infty} \hat{\boldsymbol{z}} \cdot \left(\boldsymbol{E}(\boldsymbol{r}) \times \boldsymbol{H}^*(\boldsymbol{r})\right)\, dx\, dy \\ &= -\frac{1}{8\pi^2}\,\mathrm{Re} \iint_{-\infty}^{\infty} \boldsymbol{E}_{xy}(\boldsymbol{k}_t, z) \cdot \left(\hat{\boldsymbol{z}} \times \boldsymbol{H}^*_{xy}(\boldsymbol{k}_t, z)\right)\, dk_x\, dk_y\end{aligned}$$

We rewrite the integrand with the wave-splitting, (2.15)

$$\begin{aligned}&-\mathrm{Re}\left\{\boldsymbol{E}_{xy}(\boldsymbol{k}_t, z) \cdot \left(\hat{\boldsymbol{z}} \times \boldsymbol{H}^*_{xy}(\boldsymbol{k}_t, z)\right)\right\} \\ &= \mathrm{Re}\left\{\frac{1}{\eta\eta_0}\left(\boldsymbol{F}^{+*}(\boldsymbol{k}_t, z) + \boldsymbol{F}^{-*}(\boldsymbol{k}_t, z)\right) \cdot \mathbf{O}^{-1}(\boldsymbol{k}_t) \cdot \left(\boldsymbol{F}^{+}(\boldsymbol{k}_t, z) - \boldsymbol{F}^{-}(\boldsymbol{k}_t, z)\right)\right\}\end{aligned}$$

Two types of components occur

$$\begin{cases} \mathrm{Re}\left(\boldsymbol{F}^{+*} \cdot \mathbf{O}^{-1} \cdot \boldsymbol{F}^{+} - \boldsymbol{F}^{-*} \cdot \mathbf{O}^{-1} \cdot \boldsymbol{F}^{-}\right) \\ \mathrm{Re}\left(\boldsymbol{F}^{-*} \cdot \mathbf{O}^{-1} \cdot \boldsymbol{F}^{+} - \boldsymbol{F}^{+*} \cdot \mathbf{O}^{-1} \cdot \boldsymbol{F}^{-}\right) \end{cases} \tag{A.1}$$

The first term in (A.1) has the form, see (2.16)

$$\boldsymbol{F}^{\pm} \cdot \mathbf{O}^{-1} \cdot \boldsymbol{F}^{\pm *} = \boldsymbol{F}^{\pm} \cdot \left(\hat{\boldsymbol{e}}_{\parallel}\hat{\boldsymbol{e}}_{\parallel}\frac{k}{k_z} + \hat{\boldsymbol{e}}_{\perp}\hat{\boldsymbol{e}}_{\perp}\frac{k_z}{k}\right) \cdot \boldsymbol{F}^{\pm *} = \frac{k_z}{k}\left(|F^{\pm}_{\parallel}|^2\frac{k^2}{k_z^2} + |F^{\pm}_{\perp}|^2\right)$$

where the projections $F_\perp^\pm$ and $F_\parallel^\pm$ are defined by $F_\perp^\pm = \hat{\boldsymbol{e}}_\perp \cdot \boldsymbol{F}^\pm$ and $F_\parallel^\pm = \hat{\boldsymbol{e}}_\parallel \cdot \boldsymbol{F}^\pm$. From (2.6), we get for $k_t \le k$

$$\left|\boldsymbol{\gamma}^\pm \cdot \boldsymbol{F}^\pm\right|^2 = \left|\hat{\boldsymbol{e}}_\parallel F_\parallel^\pm + \hat{\boldsymbol{e}}_\perp F_\perp^\pm \mp \hat{\boldsymbol{z}} F_\parallel^\pm \frac{k_t}{k_z}\right|^2 = \left(|F_\parallel^\pm|^2 \frac{k^2}{k_z^2} + |F_\perp^\pm|^2\right)$$

and we have

$$\operatorname{Re} \boldsymbol{F}^\pm \cdot \mathbf{O}^{-1} \cdot \boldsymbol{F}^{\pm *} = \left|\boldsymbol{\gamma}^\pm \cdot \boldsymbol{F}^\pm\right|^2 \frac{k_z}{k}, \qquad k_t \le k$$

Similarly for the second term in (A.1). We get ($\mathbf{O}^{-1}$ is a symmetric dyadic)

$$\begin{aligned}
&\operatorname{Re}\left(\boldsymbol{F}^{-*} \cdot \mathbf{O}^{-1} \cdot \boldsymbol{F}^{+} - \boldsymbol{F}^{+*} \cdot \mathbf{O}^{-1} \cdot \boldsymbol{F}^{-}\right) = 2 \operatorname{Re}\left(i \boldsymbol{F}^{-*} \cdot \operatorname{Im}\left(\mathbf{O}^{-1}\right) \cdot \boldsymbol{F}^{+}\right) \\
&= -2\left(\operatorname{Im}\frac{k}{k_z} \operatorname{Im}\left(F_\parallel^+ F_\parallel^{-*}\right) + \operatorname{Im}\frac{k_z}{k} \operatorname{Im}\left(F_\perp^+ F_\perp^{-*}\right)\right)
\end{aligned}$$

Finally, we get

$$\begin{aligned}
&\iint_{-\infty}^{\infty} \hat{\boldsymbol{z}} \cdot \boldsymbol{S}(\boldsymbol{r})\, dx\, dy \\
&= \frac{1}{8\pi^2 \eta\eta_0} \iint_{k_t \le k} \frac{k_z}{k}\left(\left|\boldsymbol{\gamma}^+(\boldsymbol{k}_t) \cdot \boldsymbol{F}^+(\boldsymbol{k}_t, z)\right|^2 - \left|\boldsymbol{\gamma}^-(\boldsymbol{k}_t) \cdot \boldsymbol{F}^-(\boldsymbol{k}_t, z)\right|^2\right) dk_x\, dk_y \qquad \text{(A.2)} \\
&\quad - \frac{1}{4\pi^2 \eta\eta_0} \iint_{k_t \ge k} \left(\operatorname{Im}\frac{k}{k_z} \operatorname{Im}\left(F_\parallel^+ F_\parallel^{-*}\right) + \operatorname{Im}\frac{k_z}{k} \operatorname{Im}\left(F_\perp^+ F_\perp^{-*}\right)\right) dk_x\, dk_y
\end{aligned}$$

References

[1] A. Boström, G. Kristensson, and S. Ström. Transformation properties of plane, spherical and cylindrical scalar and vector wave functions. In V. V. Varadan, A. Lakhtakia, and V. K. Varadan, editors, *Field Representations and Introduction to Scattering*, Acoustic, Electromagnetic and Elastic Wave Scattering, chapter 4, pages 165–210. Elsevier Science Publishers, Amsterdam, 1991.

[2] N. E. Buris, T. B. Funk, and R. S. Silverstein. Dipole arrays printed on ferrite substrates. *IEEE Trans. Antennas Propagat.*, **41**(2), 165–176, February 1993.

[3] A. L. P. S. Campos, M. A. B. Melo, and A. G. d'Assunção. Frequency-selective surfaces with rectangular apertures on uniaxial anisotropic substrates. *Microwave Opt. Techn. Lett.*, **25**(2), 126–129, April 2000.

[4] T. K. Chang, R. J. Langley, and E. A. Parker. Frequency-selective surfaces on biased ferrite substrates. *Electronics Letters*, **30**(15), 1193–1194, 1994.

[5] T. A. Cwik and R. Mittra. The cascade connection of planar periodic surfaces and lossy dielectric layers to form an arbitrary periodic screen. *IEEE Trans. Antennas Propagat.*, **35**(12), 1397–1405, December 1987.

[6] T. A. Cwik and R. Mittra. Correction to "The cascade connection of planar periodic surfaces and lossy dielectric layers to form an arbitrary periodic screen". *IEEE Trans. Antennas Propagat.*, **36**(9), 1335, September 1988.

[7] T. Ege. Scattering by a two dimensional periodic array of conducting rings on a chiral slab. *IEEE Antennas and Propagation Society International Symposium*, **3**, 1667–1670, 1996.

[8] A. Ishimaru. *Electromagnetic Wave Propagation, Radiation, and Scattering.* Prentice-Hall, Inc., Englewood Cliffs, New Jersey, 1991.

[9] A. Karlsson and G. Kristensson. Electromagnetic scattering from subteranean obstacles in a stratified ground. *Radio Sci.*, **18**(3), 345–356, 1983.

[10] A. O. Koca and T. Ege. Effects of chiral loading on a frequency selective surface comprised of a two dimensional array of crossed dipoles. *IEEE Antennas and Propagation Society International Symposium*, **2**, 1464–1467, 1996.

[11] A. O. Koca and T. Ege. The reflection and transmission characteristics of a frequency selective surface comprising of crossed dipoles on a chiral substrate. *Electrotechnical Conference MELECON '96, 8th Meditarranean*, **1**, 531–533, 1996.

[12] G. Kristensson. Electromagnetic scattering from buried inhomogeneities—a general three-dimensional formalism. *J. Appl Phys.*, **51**(7), 3486–3500, 1980.

[13] G. Kristensson. The electromagnetic field in a layered earth induced by an arbitrary stationary current distribution. *Radio Sci.*, **18**(3), 357–368, 1983.

[14] G. Li, Y. Chan, T. Mok, and J. Vardaxoglou. Analysis of frequency-selective surfaces on a biased ferrite substrate. *Int. Journal of Electronics*, **78**(6), 1159–1175, 1995.

[15] G. Li, Y. Chan, T. Mok, and J. Vardaxoglou. Analysis of frequency selective surfaces on biased ferrite substrate. *IEEE Antennas and Propagation Society International Symposium*, **3**, 1636–1639, 1995.

[16] Y. Liu, C. G. Christodoulou, and P. F. Wahid. Analysis of frequency selective surfaces with ferrite substrates. *IEEE Antennas and Propagation Society International Symposium*, **3**, 1640–1643, 1995.

[17] P. M. Morse and H. Feshbach. *Methods of Theoretical Physics*, volume 2. McGraw-Hill, New York, 1953.

[18] B. Munk. *Frequency Selective Surfaces: Theory and Design.* John Wiley & Sons, New York, 2000.

[19] M. Norgren and S. He. Electromagnetic reflection and transmission for a dielectric-Ω interface and a Ω slab. *Int. J. Infrared and MM Waves*, **15**(9), 1537–1554, 1994.

[20] S. Poulsen. Scattering from frequencey selective surfaces: A continuity condition for entire domain basis functions and an improved set of basis functions for crossed dipoles. Technical Report LUTEDX/(TEAT-7073)/1–23/(1998), Lund Institute of Technology, Department of Electromagnetic Theory, P.O. Box 118, S-211 00 Lund, Sweden, 1998.

[21] S. Rikte, M. Andersson, and G. Kristensson. Homogenization of woven materials. *Archiv für Elektronik und Übertragungstechnik (AEÜ)*, **53**(5), 261–271, 1999.

[22] S. Rikte, G. Kristensson, and M. Andersson. Propagation in bianisotropic media—reflection and transmission. Technical Report LUTEDX/(TEAT-7067)/1–31/(1998), Lund Institute of Technology, Department of Electromagnetic Theory, P.O. Box 118, S-211 00 Lund, Sweden, 1998.

[23] J. Shaker and L. Shafai. Reduced angular sensitivity frequency-selective surface. *Electronics Letters*, **29**(18), 1655–1657, 1993.

[24] S. Ström. Introduction to integral representations and integral equations for time-harmonic acoustic, electromagnetic and elastodynamic wave fields. In V. V. Varadan, A. Lakhtakia, and V. K. Varadan, editors, *Field Representations and Introduction to Scattering*, Acoustic, Electromagnetic and Elastic Wave Scattering, chapter 2, pages 37–141. Elsevier Science Publishers, Amsterdam, 1991.

[25] J. C. Vardaxoglou. *Frequency Selective Surfaces (Analysis and Design).* Research Studies Press, 1997.

[26] T. K. Wu, editor. *Frequency Selective Surface and Grid Array.* John Wiley & Sons, New York, 1995.